ULTRAHIGH DETAILED BALANCE EFFICIENCIES FOR SINGLE JUNCTION SOLAR CELLS WITH STRUCTURED EMISSION

A Thesis

by

JARETT C. MARTIN

Submitted to the Office of Graduate and Professional Studies of
Texas A&M University
in partial fulfillment of the requirements for the degree of

MASTER OF SCIENCE

Chair of Committee,	Matthew Sheldon
Committee Members,	Brian Applegate
	James Batteas
	Dong Hee Son
Head of Department,	Simon North

December 2016

Major Subject: Chemistry

ABSTRACT

The promise of solar powered energy is highly attractive, generating research efforts into the physical understanding of photovoltaic devices and how a greater knowledge of these systems can be applied to improving their overall performance. The study presented here uses the model of detailed balance to calculate the efficiencies of single junction solar cells with the inclusion of angular restriction methods that rely on the anisotropic emission of ideal radiating rod shaped materials. The proposal of a device that utilizes the $\sin^2$ emission pattern of a dipole is described and adaptations of the detailed balance model are discussed for the inclusion of angular dependent restriction provided by this type of "structured emitter."

When radiative recombination is considered as the only source of energy loss, the highest efficiency a single junction cell may reach is 33.7%; however, constraining the angular range of emitted light promotes light trapping and photon recycling within the semiconductor and increases this maximum to 45.1%. Here a strategy is presented for implementing a single junction device with 60.0% efficiency, by placing anisotropic optical emitters with a dipole radiation pattern optically in-series with a conventional cell.

The analysis further considers application of so called "structured emission" to the inclusion of non-radiative losses incurred by real material properties of GaAs. The Auger losses of GaAs systems are dominant in power conversion efficiencies; however, a broadening in the range of maximum efficiency results

from the modified emission and implies less reliance on external optics to track the maximum intensity of the sun. This increase in maximum efficiency angles allows for less intensive solar tracking, which can be reflected in decreased device complexity and cost.

Additionally, real material properties of nanocrystal photoluminescence are described with a bandwidth addition to the band gap of the cell. For Auger-limited GaAs cells, nanorod inclusion provides a linear decrease in efficiency associated with the decreased absorptivity occurring in the near band gap region. Arbitrary band gap cells are limited to the best angle restricted efficiency commonly reported; however, they show a trend of decreasing band gap shifts for the point at which maximum efficiency occurs.

ACKNOWLEDGEMENTS

I would like to thank my committee chair, Dr. Sheldon, and my committee members, Dr. Applegate, Dr. Batteas, and Dr. Son, for their guidance and support throughout the course of this research. Dr. Sheldon showed great patience and provided encouraging advice as needed, and for that I am grateful.

I would also like to thank my friends, colleagues, and the department faculty and staff for making my time at Texas A&M University a great experience. Specifically, I would like to thank students in the Sheldon lab group for making my last year as a graduate student enjoyable and entertaining. Additionally, I wish to thank Cody Chalker for his help in academic regards and general support during times of stress and need. Similarly, I wish to thank Brian Young and Meagan Elinski for their support during my time at A&M.

I want to recognize the Welch Foundation for providing funding for this project and my time as a graduate student.

Finally, thanks to my mother and father for their encouragement and support throughout my life and career as a student. Without their continual support, drive, and acceptance, I could not have accomplished my goals.

TABLE OF CONTENTS

Page

LIST OF FIGURES

FIGURE Page

FIGURE Page

LIST OF EQUATIONS

EQUATION Page

LIST OF TABLES

TABLE Page

1. INTRODUCTION

1.1 Current State of Photovoltaics

World energy production remains dominated by non-renewable sources; however, the technology behind renewable energy sources including solar, geothermal, and wind have steadily improved and began to challenge the economic viability of our dependence on hydrocarbon fuels. The sun is by far the most abundant energy source available to man providing approximately 1.2 x 10^5 TW of energy to the earth per hour, dwarfing the estimated total world energy consumption of.[1,2] Solar energy production has continued to increase in recent decades reaching a global contribution of an estimated 178 GW of photovoltaic (PV) capacity, equivalent to supply about 1% of the global energy consumed in 2014.[1,3] Continued improvements in solar materials have decreased solar energy prices, with U.S. estimates between $1.80 - 3.30/W for utility scale and residential applications respectively in 2014.[3] This is a drastic improvement from prices exceeding $70/W with the conception of PV devices in the 1970's. While this is still far above current U.S. electricity rates at 10's of cents per kWh, the decreasing PV energy costs could potentially rival conventional carbon based energy sources in the near future.[4]

There are a number of ways to decrease the cost of PV's. Some of the major financial considerations include raw semiconductor and device materials, installation, governmental incentives provided, and improved PV performance with increased device efficiencies. In recent years, silicon prices have hit all-time lows as Asia, in particular China, has begun to manufacture large quantities of silicon solar cells and PV's.[5] With a

market becoming increasingly saturated with silicon PV devices, the reality of significant price reduction from cheaper materials alone may not be the most viable solution to achieving cheaper PV's. As atmospheric pollutant levels continue to rise, regional and national incentive programs for installing and utilizing PV devices continue to encourage individuals to opt for solar energy by providing tax breaks that aid in offsetting the initial installation and start-up costs. While these incentives are beneficial, it is likely that they will begin to decline as more energy is derived from renewable energy sources. Thus, one of the more promising avenues to reducing solar energy cost's is by designing new PV's and solar cells with greater efficiency of converting solar energy into electrical energy output.

One of the underlying issues of silicon photovoltaic devices is their lack of power conversion efficiency. Commercial silicon PV devices currently operate at 10-15% efficiency depending on the manufacturer, design, and intended use of the module.[6] Monocrystalline silicon lab cells have efficiencies exceeding 20% (as noted below), however the research techniques used in the laboratory are not suitable for commercial production within the photovoltaic industry, therefore lower cost techniques (resulting in lower efficiency) are used. While commercial modules operate at lower efficiencies, the record efficiency monocrystalline silicon lab cell was recently set at 25.6%, utilizing Panasonics's HIT heterojunction of Si:H and a crystalline Si wafer.[7] Unfortunately, this efficiency value is only six tenths of a percent higher than the previous record for Si cells, set in the late 1990's, indicating a potential plateau in reaching higher efficiencies for monocrystalline Si.[8] Monocrystalline Si cells utilizing light concentrator concepts

experience slight improvements in efficiency values, with record efficiency at 27.6%, demonstrating only minor improvements over previous concentrated cell efficiencies.[7] An alternative to crystalline cells has been the use of Si thin film technologies, providing distinct advantages in their flexibility and application to non-traditional surfaces, although they suffer from decreased efficiencies (typically < 10%).[9,10]

Fortunately, Si is not the only capable material for use in solar applications. Other semiconducting materials including GaAs, GaInP, InP, CdTe, $Cu(In,Ga)(Se,S)_2$ (CIGS), and a variety of multijunction combined semiconductors have been used achieving higher efficiency values compared to traditional Si cells.[11,12,13] One of the most promising single junction species are monocrystalline GaAs cells, reaching a record efficiency of 28.8%, the highest efficiency achieved for any monocrystalline material.[6] GaAs cells have a band gap energy (1.42 eV) that matches well with the maximum energy range of the sun, in addition their advantages over Si cells include a direct band gap, decreased loss pathways, and high absorption coefficients. Achieving the greatest efficiency values are multi-junction cells that use combinations of different semiconducting materials connected in series, allowing greater utilization of incoming light. Many multi-junction cells have recorded efficiency values exceeding 30%, with the current overall record holder for all solar cells composed of a four-junction cell with an efficiency value of 46.0%.[14] While multi-junction cells achieve greater efficiency values compared to traditional monocrystalline cells, they require more time and resources to fabricate and tend to have less versatility in their applications.

Besides using different semiconducting materials, researchers are continually looking for ways to improve upon solar cell technology by making them more efficient and versatile. Many optical methods have been employed to cells, including the use of lenses over or surrounding the cell acting to either increase the angular range of light on the cell (concentration) or reduce the amount of light leaving the cell (restriction) upon reemission. These optical schemes are some of the most common methods used to improve cell efficiencies, increasing currents and voltages within the cell, but require tracking devices and specialized filtering lenses.[15,16,17,18] Other methods involve physical alteration to the semiconductor surface and application of designed geometries to the cell surface.[19,20,21] Surface texturing of the semiconductor has been used to increase the amount of photons trapped within a cell and increase the overall path length of absorption according to the $4n^2$ Yablonovitch limit.[18,22,23] By increasing the time a photon spends within the semiconductor, the probability of absorption and conversion into energy is increased. Other surface applications include applying mirrors or reflective surfaces to the rear of the cell, also increasing the photon path length within the cell.[17,24]

Recently, methods of using nano-materials and photonic crystals have been integrated into solar cells, aiming to utilize their unique properties and enhance cell function through greater absorption and improved photon extraction. Nanomaterials have highly tunable properties such as size, shape, and quantum efficiencies, lending themselves as natural candidates to inclusion with PV devices for next generation solar cells. Applications include taking advantage of the nano-material properties such as

improved light plasmonic effects[25,26], light scattering[27], and carrier extraction through hot carrier excitation[28,29], enabling further enhancement of the PV device, while other approaches look to bring the semiconductor itself to the nanoscale such that its inherent quantum properties may be explored.[30,31]

The search for greater efficiency PV's is ongoing and involves many different methods as outlined above. In the study considered here an angle restricted approach is applied through the design of a theoretical device which relies on anisotropic dipole radiators. To follow, these methods are outlined and the corresponding mathematics discussed for modeling the proposed device.

1.2 Theoretical Efficiency Considerations

Many of the methods used to improve solar cell efficiency have been derived from theoretical considerations and calculations based on the underlying physics governing the semiconducting materials. In 1961, William Shockley and Hans Queisser published a method using the thermodynamic principles of detailed balance to describe the physics of an absorbing semiconductor solar cell, predicting a maximum power conversion efficiency of approximately 30%, known as the Shockley Queisser (SQ) limit or alternatively the detailed balance limit.[32] This original study used detailed balance methods to describe current and voltage characteristics of a given semiconductor that absorbed and emitted radiation as a blackbody energy source. Since their initial study, simulated solar spectra based on experimentally collected solar data have been implemented to yield a maximum efficiency value of 33.7% under the AM 1.5G

spectra.[33] These efficiency limits, along with the corresponding record efficiencies for select semiconducting materials mentioned in section 1.1, are plotted in Figure 1. The detailed balance limit remains the "gold standard" for solar efficiency comparisons as it has yet to be surpassed by modern single junction solar cells. Additionally, the formalism of detailed balance provides a systematic mathematical method that can effectively model the characteristic physical performance of a solar cell. Many researchers have since expanded on the original SQ detailed balance method, using it as a model and starting point for generating new approaches to reduce loss within the cell and increase its efficiency.

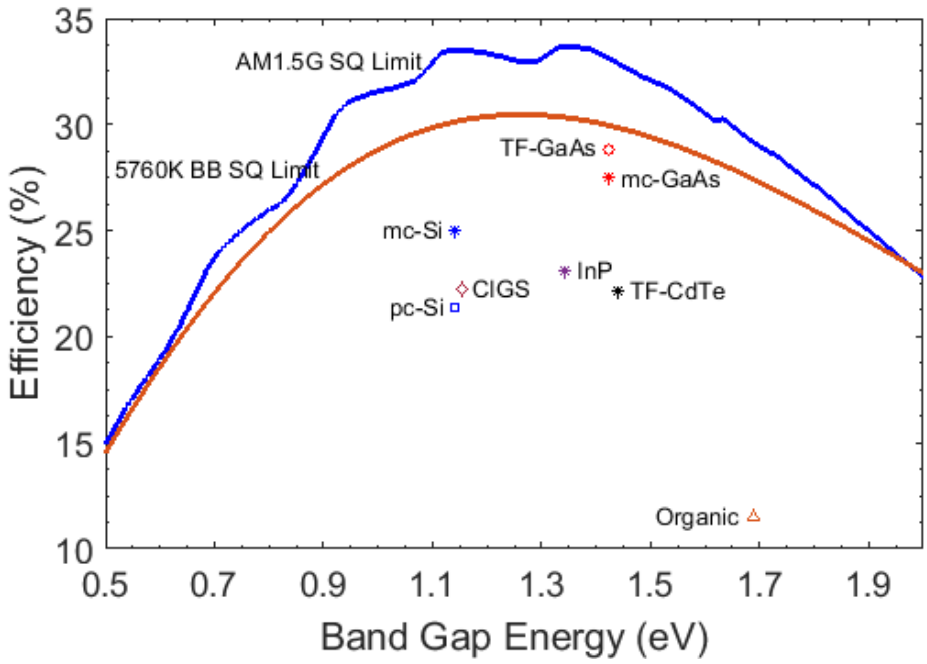

Figure 1.1. Plot of band gap energy vs. efficiency values showing the detailed balance limits for a 5760K blackbody (BB) emitter (red line) and the AM 1.5G solar spectra (blue line). Also shown are record efficiency values for various solar cell materials under non-concentrated light applications. The different types of applications are denoted as follows: mc is mono-crystalline, pc is poly-crystalline, TF is thin film.

1.3 Basic Solar Cell Physics

The solar cell is the simplest building block of a photovoltaic device, whereby multiple cells are connected in series to generate a usable output voltage. A cell acts like a two terminal device conducting as a diode in the absence of light and generating a photo-voltage when light is applied. Exposure of the cell to light generates a photo-voltage, due to the photovoltaic effect, where energy in the form of photons cause electrons to be promoted into an excited state, these electrons may then be extracted through a conductive junction to power a load in an external circuit. The process of bandgap excitation is shown for a general semiconducting material in Figure 1.2 (A), demonstrating the excitation of electrons from the valence band to the conduction band where they may be extracted, while the holes from which the electrons were ejected in the valence band remain behind, generating a potential bias. In a typical silicon solar cell a combination of negatively doped (n-type) silicon and positively doped (p-type) silicon are tightly bound together. The excess electrons in the n-type silicon migrate to fill the excess holes in the p-type silicon, this action generates a barrier to continued electron migration at their junction and a fixed electric field is created upon reaching equilibrium. When the cell is subjected to energy in the form of photons, electrons are again free to move and those close to the barrier region are swept by the existing electric field into the n-type silicon and may be extracted as a voltage, while the holes remaining can be refilled by electrons when connected to an external circuit, such that current flows in only one direction. A general schematic of this process for a typical Si solar cell is shown in Figure 1.2 (B).[34] This brief explanation of an operational solar cell is meant to

provide a brief background of the operating principles; however, detailed discussion of solar cell engineering can be found in many standard textbooks which are outside the context of this study.

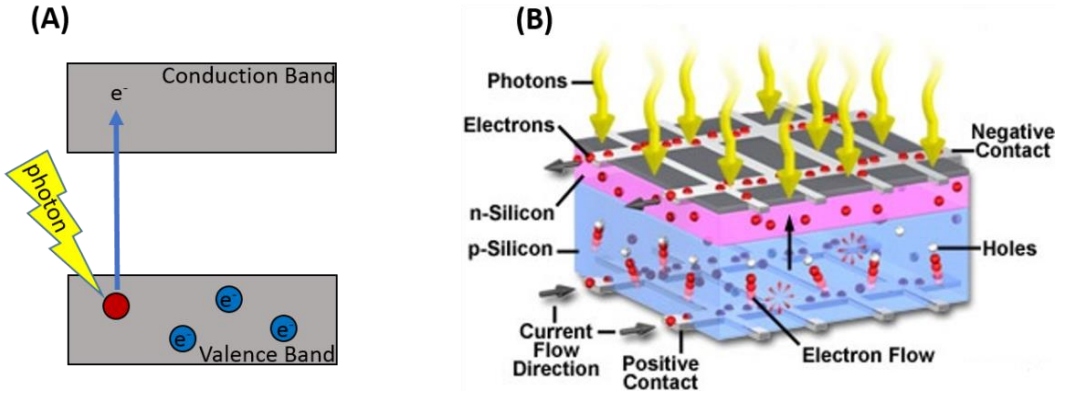

Figure 1.2. A) Diagram showing the promotion of an electron from the valence band of a semiconductor into the conduction band, B) schematic representation of a typical silicon solar cell showing the flow of current and voltage through the contacts, caused by photon induced electron movement. Figure 1.2 (B) is reprinted with permission from Molecular Expressions.[34]

A solar cell is similar to a battery in an electric circuit. In the dark, no current or voltage is produced in the circuit, however when light is applied the circuit is switched on and a voltage is generated, analogous to the e.m.f. generated in a battery, shown in Figure 1.3.[35] The voltage created when the terminals are isolated is known as the open circuit voltage (V_{oc}), and the current drawn when the terminals are connected is known as the short circuit current (I_{sc}). Any intermediate load resistance R in the cell creates a voltage V and delivers a current I, whereby Ohms law, V=IR, is established and I(V) can be determined by the current-voltage characteristic of the cell under illumination.[35] These processes and terms can then be represented using mathematics based on the

interaction with a light source and are critical in the understanding and explanation of detailed balance in a solar cell.

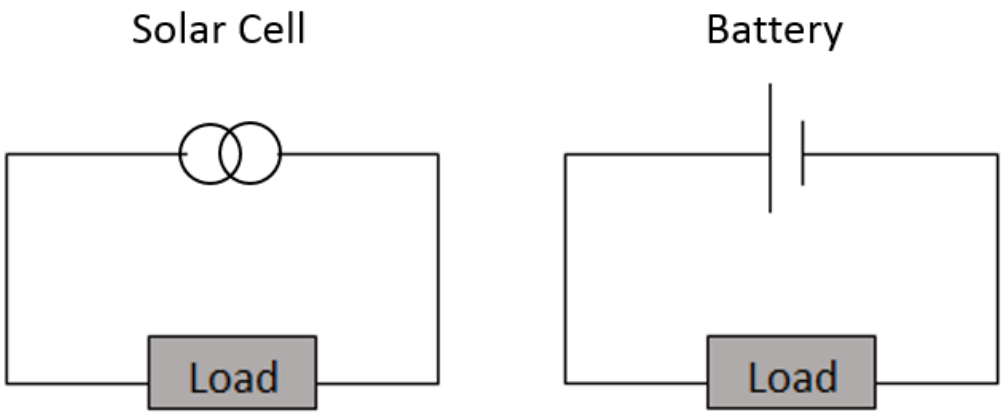

Figure 1.3. The solar cell can take the place of a battery in a simple electric circuit. This figure was reprinted with permission.[35] Copyright 2003 Imperial College Press.

2. THEORETICAL CONCEPTS

2.1 Detailed Balance and the Shockley Queisser Limit

Standard thermodynamic theory states that a system in thermodynamic equilibrium is achieved only when the conditions of detailed balance are met. The conditions of detailed balance are summed, whereby every process that occurs in a system must be balanced by its inverse. Under these conditions there is no net effect felt on the system. The detailed balance approach can be applied to semiconducting solar cell materials by considering the energy entering or leaving the cell in the form of photons. The energy entering and leaving the cell must remain in equilibrium, and as such, the light entering the cell must be equivalent to that which is leaving it, under the condition that no other load is connected to the cell.

Photons emitted from the sun act as the energy source incident on a solar cell, where the sun can be described as a blackbody emitter. A blackbody emits energy with a distribution determined solely by its temperature. The sun is considered a perfect blackbody with a temperature of 5760 K, emitting light into wavelength ranges covering the ultraviolet, visible, and infrared regions of the electromagnetic spectrum.[35] Using Planck's law of blackbody radiation, a blackbody source can be mathematically described in its wavelength equivalent form as:

$$B_\lambda(\lambda, T) = \frac{2hc^2}{\lambda^5} \frac{1}{e^{\frac{hc}{\lambda k_b T}} - 1} \tag{2.1}$$

where λ is the wavelength of light in nanometers, T is the temperature of the emitting body in Kelvin, h is Planck's constant, c the speed of light, and k_b is the Boltzmann constant.[36] While this form of the equation is useful for describing the sun's emission based on its varied intensity per given wavelength, it becomes easier to describe light as quanta of energy. Equation (1.1) can be converted to its energy equivalent form using the relation $E = \frac{hc}{\lambda}$, resulting in

$$B_E(E,T) = \frac{2}{h^3c^2}\frac{E^2}{e^{\frac{E}{k_bT}} - 1} \tag{2.2}$$

In a solar cell the bias (V) created by the excitation of excess charge carriers is known as the chemical potential (μ) and can be shown as $\mu = qV$, where q is the charge of the carrier. The number of photons in a given mode of radiation is given by the Bose-Einstein factor, $f_{BE} = \left\{exp\left[\frac{(E-\mu)}{k_BT}\right] - 1\right\}^{-1}$,and can be substituted into Equation (2.2) to account for the potential occurring within the cell.[37] The blackbody expression shown in Equation (2.2) can be used to calculate the quantity of light both absorbed and emitted by a cell.

The simulation of a solar cell can be described as both an absorber and emitter of radiation using the blackbody flux, whereby in the emissive case the potential occurring within the cell is included as a voltage (V). The rate of photon absorption incident on the cell can be calculated as, N_{abs},:

$$N_{abs}(\theta_{Sun}, E, T) = \int_{E}^{\infty} \int_{\varphi=0}^{2\pi} \int_{\theta=0}^{\theta_{Sun}} a(\theta, \varphi, E) B(E, T) cos\theta sin\theta d\varphi d\theta dE \tag{2.3}$$

where the incident energy is integrated over all angles of light received from the sun, $0° \rightarrow \theta_{Sun} = 0.267°$. The angular dependent absorptivity of the cell, $a(\theta, \varphi, E)$, quantifies the fraction of photons at energy, E , and incident angles, θ and φ, absorbed by the cell. Similarly the number of photons emitted per unit time can be described by N_{emit}, shown as:

$$N_{emit}(\theta_{emit}, E, V, T) = \int_{E}^{\infty} \int_{\varphi=0}^{2\pi} \int_{\theta=0}^{\theta_{emit}} e(\theta, \varphi, E) B(E, T, V) cos\theta sin\theta d\varphi d\theta dE \tag{2.4}$$

where the light emitted from the cell is due solely to radiative recombination. The emission flux N_{emit} is defined in terms of the generalized Planck distribution for a blackbody over a range of energy $E_g \rightarrow \infty$, where only photons with energy greater than the band gap energy, E_g, are emitted. The voltage dependence as described above is due to the chemical potential the cell possesses after absorption of incident light. Using the principal of detailed balance, the absorption and emission fluxes are set equal to one another at equilibrium and Equation (2.5) may be established.

$$N_{abs}(\theta_{Sun}, E, T) = N_{emit}(\theta_{emit}, E, V, T) \tag{2.5}$$

With the flux of photons into and out of the semiconductor described, one can now determine the current and voltage characteristics occurring within the cell. The detailed balance limit has a few key assumptions that idealize and simplify the efficiency determination of the cell. First, it is assumed that for every photon absorbed by the cell with energy above the band gap, one electron-hole pair is generated. Second, the cell is operating in the radiative limit, such that only radiative recombination is considered and non-radiative losses are ignored. Third, the cell is operating under non-concentrated one-sun illumination. The final assumption for maximum efficiency calculations in the detailed balance limit is that all generated charge carriers are collected as current, or recombine, emitting a single photon for each electron-hole pair. With these assumptions the total current density in the cell can be calculated as:

$$J_{tot} = q\big[N_{abs}(\theta_{Sun}, E, V = 0, T_{Sun}) + N_{amb}(\theta_{emit}, E, V = 0, T_{cell}) - N_{emit}\big(\theta_{emit}, E, V_{app}, T_{cell}\big)\big] \tag{2.6}$$

where the middle term, N_{amb}, is the absorption from the emission of ambient surroundings; however, it is much smaller than the absorption contributed by the sun.[38] When calculating the total current density, the voltage term in the emission flux is due to an applied voltage and is shown as V_{app}. Equation (2.6) is essential in calculating limiting current and voltage cases in the cell and can be further manipulated to distinguish where individual currents are originating. The light generated current density is given by:

$$J_L = N_{abs}(\theta_{Sun}, E, V = 0, T_{Sun}) \tag{2.7}$$

which represents the limiting case within the cell when no voltage is present and thus is commonly termed the short circuit current, J_{sc}. The dark current density, in the radiative limit, is given by

$$J_0 = J_R\left[e^{\frac{qV}{k_bT}} - 1\right] = N_{emit}\left(\theta_{emit}, E, V_{app}, T_{cell}\right) - N_{amb}(\theta_{emit}, E, V = 0, T_{cell}) \tag{2.8}$$

where J_R is the reverse saturation current and representative of the recombination current generated within the cell.[38]

In the limiting case where no current is extracted from the cell, the cell is said to be at open circuit conditions. The open circuit voltage, V_{oc}, of the cell is obtained from Equation (2.6) by setting the current to zero, replacing V_{app} with V_{oc} and solving for the voltage as

$$V_{oc} = \frac{k_bT_{cell}}{q}\ln\left(\frac{J_{sc}}{J_R} + 1\right) \cong \frac{k_bT_{cell}}{q}\ln\left(\frac{J_{sc}}{J_R}\right) \tag{2.9}$$

where the $\frac{k_bT_{cell}}{q}$ term represents the thermal voltage of the cell and V_{oc} is effectively a representation of the ratio of light generated current to recombination current.

With relevant current and voltage terms defined, the efficiency of the cell can be determined by plotting the JV curve generated by the cell and finding the maximum

current and voltage points, J_{opt} and V_{opt}, of the curves apex. Another common way of representing the efficiency is by defining a fill factor of the cell, which describes how square the JV curve is at its maximum operating J and V points, and multiplying this factor by the $J_{sc}$and V_{oc} . The fill factor is shown as:

$$FF = \frac{J_{opt}V_{opt}}{J_{sc}V_{oc}} \tag{2.10}$$

and with it the efficiency of the cell, η, can now be shown by dividing the maximum operating power, P_{max}, by the incident power, P_{inc}, in conjunction with the J_{sc} and V_{oc} terms.

$$\eta = \frac{J_{sc}V_{oc}}{P_{inc}}FF = \frac{P_{max}}{P_{inc}} \tag{2.11}$$

By defining the cells voltage and current characteristics in this manner to solve for the cells efficiency, Shockley and Queisser were able to calculate the maximum efficiency possible for a semiconducting material to be 30.5% at a band gap energy of 1.31 eV.[32]

2.2 Applying Real Solar Spectra

Equation (2.3) provides a quantitative approach to calculating the amount of photons per unit time a cell may absorb based on its energy, temperature, and the angle

of incidence of the blackbody. However, this calculation is only an approximation of our sun, not a direct representation, as it fails to account for the full energy dependent intensity the sun has at differing wavelengths. The number of photons per unit time received from the sun, known as solar irradiance, is shown as a function of wavelength using experimentally collected reference data in Figure 2.1. Close inspection of Figure 2.1 reveals similarities between the blackbody flux calculated using Equation (2.3) and the ASTM reference spectra, with maximum intensity occurring in the visible region of the spectrum. The major differences in theses fluxes lies in the failure of the blackbody curve to account for gas absorption bands, caused largely by carbon dioxide (CO_2), water (H_2O), and ozone (O_3) present in Earth's atmosphere. The major absorption bands for each are around 500 nm for O_3, the large dips around 1400 nm and 1900 nm originating from combinations of CO_2 and H_2O, and the rest of the dipping absorption bands due to water.[39] The reference spectra given by NREL are designated by air mass (AM), which simply quantifies the reduction in the power of light as it passes through the atmosphere and is absorbed by air and dust.[40] The air mass zero (AM 0) extra-terrestrial spectrum corresponds to the intensity of photons felt just outside the atmosphere of the earth, while the air mass 1.5 direct normal (AM 1.5), more commonly referred to as AM 1.5D, spectrum represents the intensity of photons felt at sea level.[33]

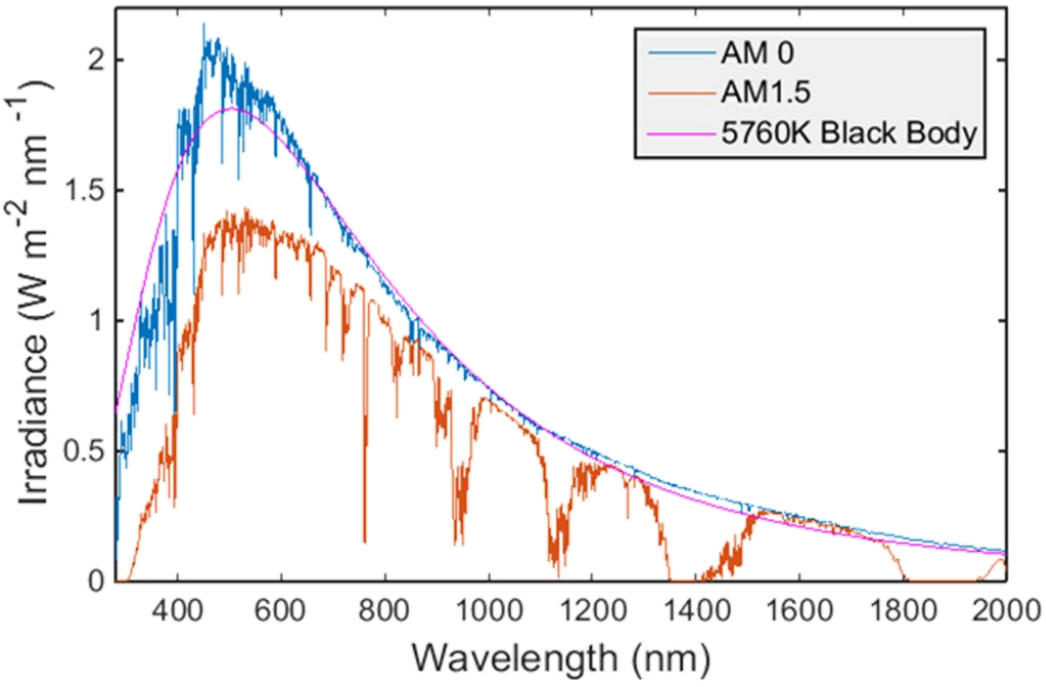

Figure 2.1. Plots of solar irradiance for the extra-terrestrial (AM 0) spectrum (blue line), the direct normal (AM 1.5) spectrum (red line), and a black body emitter at a temperature of 5760K (pink line).

The two terrestrial reference spectra recognized as standards for solar related works are the AM 1.5D as shown above and the AM 1.5G, air mass global. The significance of differentiating between which of these is used for simulations depends on the conditions of which the solar device is being exposed to. As will be described in chapter 3 the AM 1.5G is best suited for use in normal simulations and tests of solar devices, where sunlight is received from all angles along with diffuse reflected light. The AM 1.5D spectrum is used when the solar device is designated to receive light directly from the sun and all diffuse light is to be ignored, such is the case when concentrating or restricting optics, discussed in section 3.1, are applied to the cell.

With reference spectra given, realistic calculations for solar cell absorption can be performed by substituting $B(E,T)$ in Equation (2.3) with the desired spectra represented by the term $S(E)$.

$$N_{abs}(\theta_{Sun},E,T)=\int_{E}^{\infty}\int_{\varphi=0}^{2\pi}\int_{\theta=0}^{\theta_{Sun}}a(\theta,\varphi,E)S(E)cos\theta sin\theta d\varphi d\theta dE \tag{2.12}$$

The inclusion of the solar spectrum into the absorption flux equation allows for more accurate simulations and was shown using the AM 1.5G data in the detailed balance limit calculation in Figure 1.1.

3. STRUCTURED EMISSION AND DETAILED BALANCE

3.1 Solar Concentration and Emission Angle Reduction

To increase the efficiency of the cell one of the most common utilized techniques is to apply concentrated light to the cell. This approach relies on using lenses and optics to focus light onto the cell, therefore broadening the incident angular range and increasing the intensity of light on the cell surface. In a typical cell light is received from the small angular range spanned by the solar disk, where the half-angle received from the sun is $\theta_{Sun} = 0.267°$. The energy striking a surface within this angular range is equivalent to ~ 900 W/m^2 for the AM 1.5D spectrum and ~ 1000 W/m^2 for the AM 1.5G spectrum, where the equivalence of a one-sun concentration factor is set to be 1000 W/m^2.[41] Therefore, to increase the concentration of sunlight on the cell, lenses and parabolic mirrors may be placed around the cell so that a larger angular range of light is applied to the cell, similar to a magnifying glass. As a result, the efficiency increases as the absorption flux from Equation (2.2) increases, sequentially causing a rise in the light generated current.

A theoretical concentration limit equivalent to, termed 'perfect concentration', can be achieved through concentration where $\theta_{Sun}$is expanded to equal θ_{emit}.[42,43] The enhanced flux from concentration increases current density from the cell, and can increase efficiency to a theoretical maximum of 45.1% for a band gap energy of 1.12 eV.[44] In practice however, concentration values above a few hundred suns generate excessive current densities that result in deleterious heating of the cell, increased series resistances, and loss of efficiency.[45,46] In addition, concentration schemes require

mechanical trackers to follow the sun's position throughout the day that can significantly increase the cost of PV modules.[15]

Alternatively, according to the equality in Equation (2.5), limiting the angular range of light leaving the cell, θ_{emit}, through the use of angle restriction optics can also increase the voltage and efficiency of the cell. Typically light is re-emitted isotropically into a larger angular range, where the emission angle spans from $0° \rightarrow \theta_{emit} = 90°$. This greater angular range of θ_{emit}, compared to θ_{Sun}, results in an entropic loss to the cell and limits cell efficiency. In contrast to concentrator optics, restriction strategies preserve the angular range of light received from the sun, while the angular range of light reemitted is constrained using mirrors or directionally selective reflective filters, effectively trapping light and recycling photons within the cell that would otherwise be sent to more oblique angles outside the cell.[47,48,49,50,51] At steady state, the increased number of trapped photons increases the V_{oc} of the cell, while J_{sc} remains unaffected. Perfect restriction optics, where $\theta_{emit} = \theta_{Sun}$, can provide the same theoretical efficiency maximum as perfect concentration without the deleterious heating due to increased current densities. However, this strategy requires semiconductor materials that are highly efficient radiative emitters, and still requires precision tracking to maintain alignment between the sun and the optical path to the cell.[51,52] As noted by other researchers, the enhanced V_{oc} provided by both concentrators and angle restriction optics can be understood as resulting from the net decrease of the angular entropy associated with the photons re-emitted from the cell compared with a conventional flat-plate geometry.[47,49,53,21]

3.2 Angle Restriction and Design of a Structured Emitter

Building from the angular restriction strategies outlined above, the modification of the angle dependent emission intensity may be addressed and shown to benefit conversion efficiency. That is, even if a solar cell emits radiation isotropically into the same angular range as a conventional flat-plate cell, $\theta_{emit} = 90°$, the light trapping that can result by structuring the intensity profile of that emission can be analyzed. This could be achieved practically, for example, by placing optical emitters with anisotropic radiation intensity patterns optically in-series between the cell and the sun, shown in Figure 3.1 (B), in order to redirect the angular occupation of the emitted radiation. There is special interest in this effect as it relates to the anisotropic dipolar emission provided by highly luminescent rod-shaped semiconductor nanocrystals[54,55,56]. In nanorods, differences in the quantum confinement of electronic states along the short and long dimensions promote linearly polarized band-edge luminescence with intensity that is maximized normal to the long axis.[57] These nanorods emit comparably to an antenna and as such have an emission pattern well described by a $\sin^2$ distribution, shown by the blue torroid pattern in Figure 3.1 (A).

Several researchers have proposed the use of aligned nanorods, or other linearly polarized fluorophores, to enhance the performance of luminescent solar concentrators (LSCs) by preferentially reemitting radiation into waveguide modes that couple to the PV element.[58,59,60] With this body of work in mind, the proposal of a similar type of structure was devised and is shown in Figure 3.1 (B). The proposed structure utilizes aligned dipole radiators emitting into a waveguide medium containing a PV element. As

shown, the PV element is completely surrounded by mirrors, assumed to be ideal reflectors, and it is assumed that the concentration of dipoles is sufficiently dense that the only light reaching the PV element is through reemitted light from the dipoles themselves. Given these assumptions, it may be concluded that the light escaping the device also exits with the same anisotropic emission pattern, described by dipole emission, and is shown in this manner on the top of the proposed device.

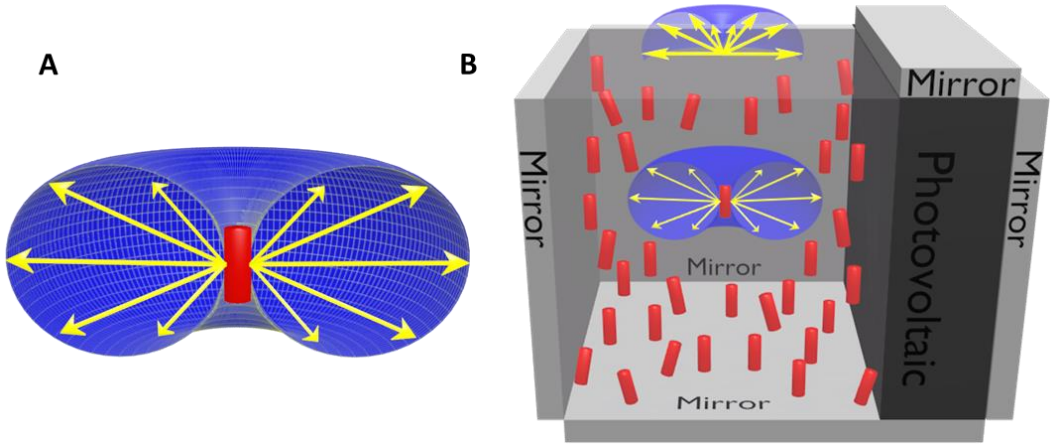

Figure 3.1. Schematic representations of A) dipole emitter and B) a proposed device structure incorporating vertically aligned dipole radiators within a dielectric medium that is optically in-series with a photovoltaic cell.

Crucially for this study, the angle dependence of the absorptivity and the band edge luminescence of a semiconductor nanorod exhibits a pronounced energy dependence.[61,62] Above band gap radiation from any incident angle will be absorbed with some efficiency, but internal electronic relaxation of excited carriers results in band-edge luminescence that is highly polarized and directed into a modified angular distribution. While details of the full spectral behavior of the optical anisotropy is strongly dependent on the composition and morphology of the nanostructure, in the best-

characterized Cd-based chalcogenide materials studied to date, the polarized absorption and emission is most pronounced for band edge states and quickly dies off at higher energies.[61,62] Thus, just as conventional semiconductors down-convert all absorbed solar radiation into band edge re-emission, nanorods additionally constrain the angular intensity profile and polarization of the band edge re-emission. The integration of nanorods into PV devices therefore represents an interesting alternative to very recent proposals for structures that do not strictly uphold optical reciprocity, i.e. time-reversal symmetry, of the angle and spectral dependence of absorption and emission of radiation during operation.[49,63] The inclusion of nanorod materials will be considered later in the manuscript and are mentioned here to provide the experimental hypothesis of how such a structured emitter may be created; however for now we assume that the dipole radiators described are unspecified ideal dipole radiators.

3.3 Modifying Detailed Balance Equations

With the proposal of structured emission through the device shown above, the manipulation to the underlying mathematics must be considered and how the emission pattern may affect the cell parameters. Assuming, for the ideal case that absorption of the device is not affected, only modifications to the emission flux from Equation (2.4) will be considered. For simplicity, an idealized flat-plate solar cell is first considered with geometry shown by Figure 3.2 (A), where it is possible to modify the angle-dependent and energy-dependent emissivity $e(\theta, \varphi, E)$ and absorptivity $a(\theta, \varphi, E)$ through some additional structure that is optically coupled to the semiconductor. The

emissivity of the cell is generally equated to the absorptivity of the cell in accordance with Kirchoff's law.[64,65] However, using materials that obey Kirchoff's law does not require that the angle dependence of the broadband absorptivity match the angular distribution of the band-edge emission, due to the energy dependence of both terms. This hypothetical optical component only modulates the relative intensity of radiation around the band edge energy, E_g, into a given angle with a weighting factor, $I(\theta, E_g)$ that can take any value between $0 \rightarrow 1$. The modified form of the emission term including this additional factor is:

$$N_{emit}(\theta_{emit}, E, V_{app}, T_{cell}) = \frac{2\pi}{h^3 c^2} \int_{E_g}^{\infty} \int_{\varphi=0}^{2\pi} \int_{\theta=0}^{\theta_{emit}} I(\theta, E_g) e(\theta, \varphi, E) \frac{E^2}{e^{\left(\frac{E - qV_{app}}{k_b T_{cell}}\right)} - 1} cos\theta sin\theta d\theta d\varphi dE \quad (3.1)$$

A dipolar re-emission pattern is described when $I(\theta, E_g) = sin^2(\theta)$ and is depicted by the surface emitting in Figure 3.2 (C). This modified emission flux decreases the emitted light by a factor of $\sin^2$ at a given angle, and thereby promotes light trapping and photon recycling. The relative decrease of emission intensity into some angles improves the overall efficiency of the cell, as the V_{oc} must increase to maintain flux balance with the sun. Note that the full energy dependence of a composite structure like that in Fig. 3.1 (B) would account for the effect of both dipolar band edge emission and absorption, and thus $e(\theta, \varphi, E) = a(\theta, \varphi, E)$ would hold as required by Kirchoff's law,

with no need to use the additional term $I(\theta, E_g)$. However, the term is included here to emphasize that the emission pattern is not an intrinsic property of the bulk semiconductor, but it is imposed by the luminescent down conversion of an in-series optical element that only exhibits dipolar absorptivity or emissivity at the band edge energy.

Using Eq. (3.1) with $I(\theta, E_g) = sin^2(\theta)$ results in a slight improvement over the flat-plate detailed balance efficiency, with a 0.6% absolute efficiency increase at the optimal band gap, as depicted in Figure 3.3 and Table 3.1. The efficiency improvement here is small, but it shows that by simply altering the emission pattern it is theoretically possible to increase overall efficiencies. This efficiency, 34.3 %, also corresponds to the highest efficiency that could be achieved with an LSC-like optical concentrator using aligned dipole sources, as depicted in Figure 3.1 (B). Note that this is a best-case estimate for the improvement that could be provided by some ideal dipole, because it assumes complete absorption of all above band gap radiation and re-emission as a perfect dipole source.

This ideal behavior is approximated by the luminescent behavior observed in recent experimental studies of Cd chalcogenide based semiconductor nanorods.[63,66] A more pronounced effect occurs when dipolar emission is combined with angle restriction optics, depicted in Figure 3.2 (B, D). For the ideal restriction case light is only emitted into the same small angular range as light is received from the sun. Figure 3.3 shows the detailed-balance efficiencies for a flat-plate cell with isotropic emission (green dashed) and the ideal angle-restriction case (red), along with the additional benefit provided by

modulation of the emission intensity with a $\sin^2$ pattern (purple and blue, respectively), assuming that the sun is normal to the cell surface. In the combined dipole-restricted case (blue) an efficiency value of 60.0% is predicted. This efficiency is significantly increased in comparison with the conventional flat-plate single junction efficiency of 33.7%.

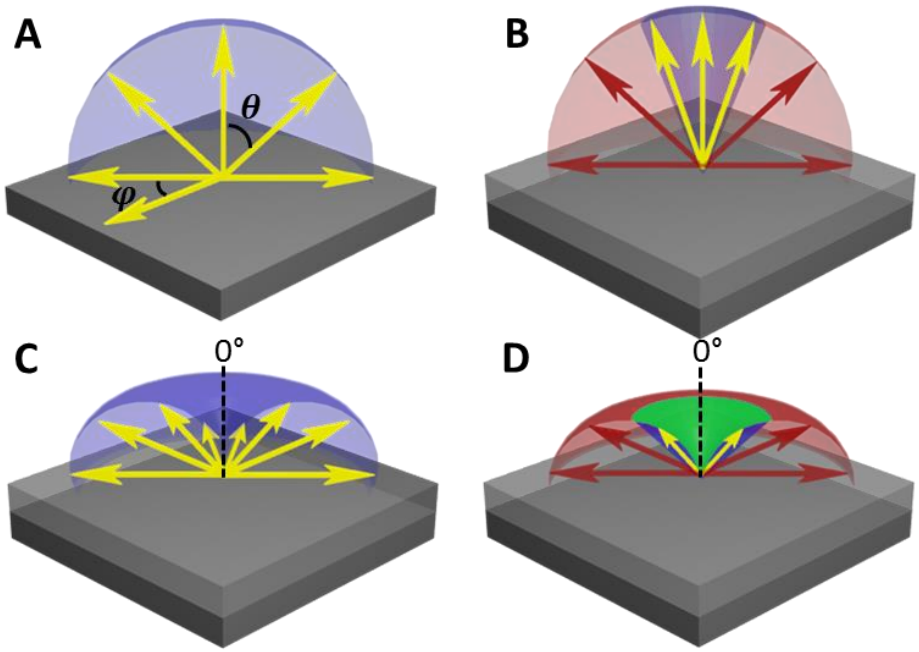

Figure 3.2. Schematic representation of the emitted radiation intensity from a single point on a solar cell surface for A) a flat-plate cell emitting isotropically into every angle equally, defined by angles θ and φ, B) restricted emission by an optical structure that allows light to leave the surface only within a narrow angular range (blue), while all other light is blocked from leaving (red), C) surface emission defined by a dipole source, exhibiting a characteristic $\sin^2$ toroid pattern into all angles, D) combined angle restriction and dipole emission, where the angular range and relative intensity of light escaping the cell has been constrained (green).

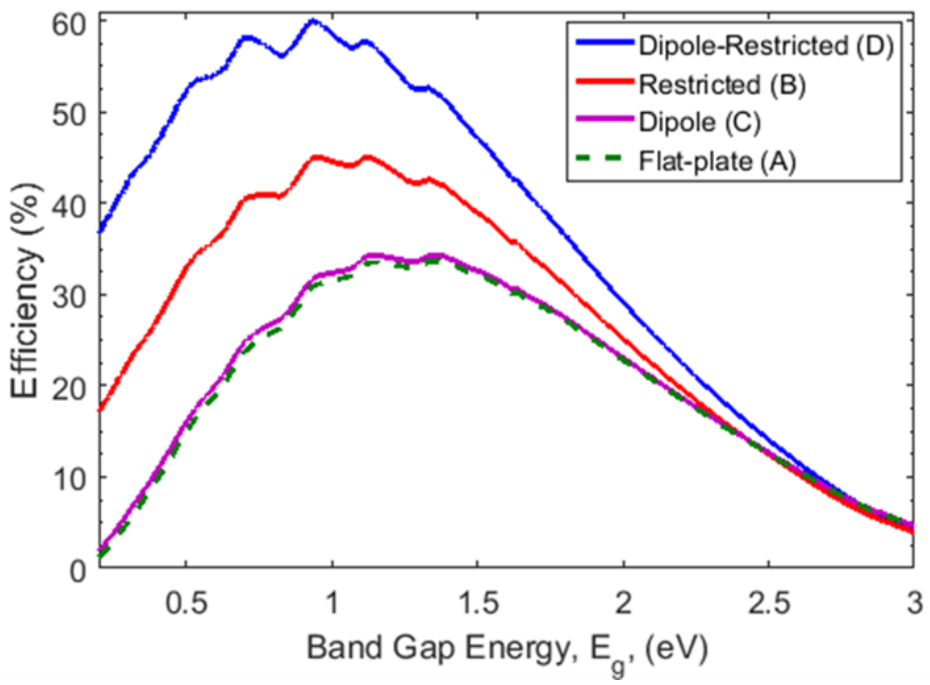

Figure 3.3. The detailed-balance efficiency as a function of band gap energy for each of the surfaces considered in Figure 3.2.

Table 3.1. The values of V_{oc} and J_{sc} at the band gap energy of the maximum efficiency point for each of the 4 cases studied in Figure 3.3. The two restricted cases use the AM 1.5D spectrum, as angle restriction requires that the cell only absorb direct sunlight. The dipole and flat-plate cases use the AM 1.5G spectrum including diffuse sunlight.

Case	Efficiency (%)	E_g (eV)	V_{oc} (V)	J_{sc} (mA/cm^2)
Flat-plate	33.7	1.34	1.08	35.2
Dipole	34.3	1.34	1.10	35.2
Restricted	45.1	1.12	1.15	39.5
Dipole-Restricted	60.0	0.93	1.27	47.1

3.4 Open Circuit Voltage and Short Circuit Current

For both angle-restricted cases, red and blue traces in Figure 3.3, the V_{oc} exceeds the band gap energy, with a significant difference in the dipole-restricted case (blue). This increase in V_{oc} is due to the greatly increased population of excited carriers resulting from the high optical concentration inside the bulk semiconductor. It is generally accepted that E_g/q defines the upper limit for V_{oc} under non-concentrated light.[66-67,68,69] When the inequality $E_g - qV \gg k_b T_{cell}$ is met, classical Boltzmann statistics are upheld and the expression for emission flux in Equation (2.9) is valid. However, under concentrated light or during angular restriction when $E_g \approx qV$, the Bose-Einstein function approaches a singularity and the ideal diode approximation fails.[37,70,71] Under these conditions the energy and exponential term in the emission flux expression of Equation (2.9) may be adapted as[37,72]

$$E^2 exp^{\left(\frac{qV_{app}-E}{k_b T_{cell}}\right)} \tag{3.2}$$

This approximation assumes that thermal equilibrium is reached among electrons in the conduction band before they relax due to band edge recombination, and corrects for the singularity when $E = qV$.[67,70,72] The approximation here is known as the van Roosbroeck-Shockley relation[72-73] and is commonly used when qV approaches E_g. The relation can be arrived at with the following approximations and manipulation.

$$e^{\left(\frac{E-qV}{kT}\right)} \gg 1 \rightarrow \frac{1}{e^{\left(\frac{E-qV}{kT}\right)}-1} \approx \frac{1}{e^{\left(\frac{E-qV}{kT}\right)}+1} \approx \frac{1}{e^{\left(\frac{E-qV}{kT}\right)}} = e^{\left(\frac{qV-E}{kT}\right)} \tag{3.3}$$

In this rearrangement the exponential term remains significantly large, as would be the case in a non-concentrated cell. This form is now similar to that of the common Boltzmann statistical function, no longer diverging when $E_g = qV$, further validating its use. Using this exponential term in the emission flux expression allows the conventional form of Equation (2.9) to be used,[37]shown below, and is implemented as required in the calculations.

$$N_{emit}\left(\theta_{emit}, E, V_{app}, T_{cell}\right) = \frac{2\pi}{h^3 c^2} \int_{E_g}^{\infty} \int_{\varphi=0}^{2\pi} \int_{\theta=0}^{\theta_{emit}} I\left(\theta, E_g\right) e(\theta, \varphi, E) E^2 exp^{\left(\frac{qV_{app}-E}{k_b T_{cell}}\right)} cos\theta sin\theta d\theta d\varphi dE \tag{3.4}$$

In addition to the increased efficiency that results from the $\sin^2$ structured emission, Table 3.1 indicates that increased light trapping provides greater efficiency improvements with smaller band gap cells. This observation is significant because some reduced band gap materials, such as germanium, indium, and lead based semiconductors[74,75], may have reduced material costs, wider availability, and can often exhibit higher quantum fluorescence yield than larger band gap analogues[31]. Additionally, the J_{sc} is nearly constant across the different geometries explored, as each

uses the same incoming flux, the AM 1.5G or AM 1.5D spectrum respectively. This suggests that devices implementing this strategy would not experience additional heating, alleviating losses that may result from increased current densities.[45-46]

Shown in Figure 3.4, the J_{sc} values for the different cases considered in Figure 3.3 are identical, depending on which spectra were used for the incident light source (AM 1.5D or AM 1.5G). This indicates there is no excessive current generation between the differing geometries and thus no additional heating would be expected to occur in the cell. The constant J_{sc} also corroborates that the rise in efficiency values is entirely due to an increased V_{oc}. Here the AM 1.5G spectra is used for the standard flat-plate cell (purple dash) and the case where the additional $\sin^2$ term is included (yellow).[3] For both of these cases it is assumed that diffuse light could be absorbed by the cell as there is no additional optical restriction. However, for both of the restricted cases (blue, dashed-red) the AM 1.5D spectra is used. Here only the direct portion of light from the sun is considered, because the angles absorbed and emitted by the cells are restricted to only the half-angles spanned by direct sunlight.[3] Observation of Figure 3.4 shows slightly higher current densities for the cases without restriction, reflected by the higher incident power resulting from the AM 1.5G spectra with a power of ~1000 W/m^2, compared to an incident power value of ~900 W/m^2 for the AM 1.5D spectra.

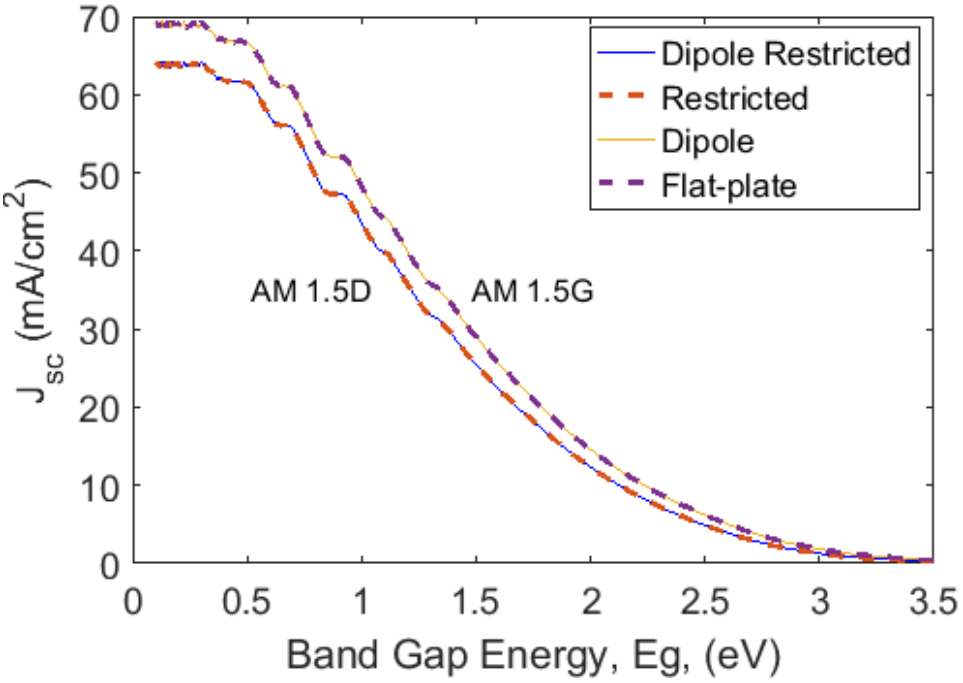

Figure 3.4. Plot of J_{sc} vs E_g for each of the 4 cases studied. Both of the restricted cases here use the AM 1.5D spectra and exhibit lower current densities, while the unrestricted cases use the AM 1.5G spectra and exhibit slightly higher current densities as a result of the increased incident power in the diffuse spectra.

3.5 Device Structure Differentiation from Luminescent Solar Concentrators

The calculated efficiencies for dipole-structured emission provide promising theoretical efficiency limits, especially when used in conjunction with angular restriction optics. To realize such a convertor device we propose an idealized LSC-like structure shown in Figure 3.1 (B). This implementation takes advantage of the dipolar emission properties of vertically aligned ideal dipole sources, which are encased in a transparent dielectric medium. The dipole medium is surrounded by perfect reflectors and optically in-series with the semiconductor, so that all light emitted at the top surface of the device exhibits a $\sin^2$ dipolar pattern (Figure 3.1 (B)). An angle restriction optic can also be

placed on the exposed top surface. A basic assumption made in this scheme is that all photons entering the device are absorbed and re-emitted by the dipole source before absorption by the PV element, and that all photons emitted from the PV element are absorbed and re-emitted by the dipole before exiting the device. Additionally, radiative emission is the only energy loss pathway present, and there is sufficient optical density of dipoles such that all incident sunlight is absorbed by the device. With these assumed limitations, Equation (3.1) and as required Equation (3.4) accurately describe the limiting device efficiency.

If geometrical concentration is present, i.e. there is a difference between the surface area of the PV element and surface area of the top of the device, J_{sc} will be modified by the concentration factor, but the device efficiency is unchanged due to the equivalent scaling of the radiative dark current, J_o, in Equation (2.9).[76] Refractive index contrast between the device structure and air similarly provides no efficiency benefit, but can increase J_{sc}.[76] The concept of perfect vertical alignment for all the dipole radiators represents a difficult engineering challenge, though there have been significant recent strides in this area.[58,77,78,79,80] Therefore calculations were performed that assumed a small amount of rotation and canting of individual rods (depicted in Figure 3.1 (B)), by setting $I(\theta, E)$ to the average value of $\sin^2$ over the angles spanned by direct sunlight. The calculated efficiency with this more realistic emissivity function is identical within the numerical accuracy of the values reported in Figure 4.1 below, where additional realistic loss mechanisms are also considered in more detail.

Although superficially similar in implementation to LSC geometries that have been proposed[58,60], it is worth emphasizing that this device geometry is not a conventional LSC, and is therefore subject to very different optimization and design constraints. Importantly, this design does not require refractive index contrast in the device structure, nor does it benefit from total internal reflection that supports waveguide modes. LSCs rely on total internal reflection that results from refractive index contrast, in order to trap light within a waveguide structure.[59,60,81,82] As required by Snell's law, the relative angle dependent emission intensity of a radiation source is not modified when crossing an interface with differing refractive indices. To follow, a derivation of Snells law is performed with the angular dependent emission intensity to prove this schemes independence of refractive index, where Figure 3.5 provides a schematic to visually aid in this derivation.

Snell's law can be used to relate the angular dependent light intensity escaping the top of the device, $I_{emit}(\theta_{emit})$, and the angular dependent light intensity within the dielectric medium that holds the anisotropic optical emitters, $I_{dipole}(\theta_{dipole})$. The dielectric medium has refractive index, n_2, and the entire structure is surrounded by air with refractive index, n_{air}. For simplicity, assume that Fresnel reflections at the interface can be neglected, as is practically achieved with anti-reflection coatings on many high efficiency solar cells. Then, the intensity of radiation emitted inside the device into a given angle θ_{dipole}, is the same as it moves across the interface into free space at an angle θ_{emit} :

$$I_{emit}(\theta_{emit}) = I_{dipole}(\theta_{dipole}) \tag{3.5}$$

where Snell's law defines θ_{emit} in terms of θ_{dipole}:

$$\theta_{dipole} = sin^{-1}\left[\frac{n_{air}}{n_2} sin(\theta_{emit})\right] \tag{3.6}$$

The intensity of the emission pattern for a dipole emitter such as a semiconductor nanorod is $sin^2(\theta_{dipole})$. Therefore, in terms of θ_{emit}

$$I_{dipole}(\theta_{dipole}) = sin^2(\theta_{dipole}) = sin^2\left(sin^{-1}\left[\frac{n_{air}}{n_2} sin(\theta_{emit})\right]\right) \tag{3.7}$$

By substituting Eq. (3.6) into Eq. (3.4), one obtains

$$I_{emit}(\theta_{emit}) = \left(\frac{n_{air}}{n_2}\right)^2 sin^2(\theta_{emit}) \tag{3.8}$$

The maximum intensity of radiation leaving the dipole emitter that can also exit the surface of the device corresponds to light that is emitted along the critical angle, θ_c, where

$$\theta_c = sin^{-1}\left(\frac{n_{air}}{n_2}\right) \tag{3.9}$$

Therefore, to obtain the *relative* intensity of light leaving the surface, $I^R_{emit}(\theta_{emit})$, Equation (3.8) must be normalized by the intensity of radiation emitted by the dipole source along θ_c inside the dielectric medium. Dividing Equation (3.7) by Equation (3.6) with $\theta_{dipole} = \theta_c$ gives

$$I^R_{emit}(\theta_{emit}) = sin^2(\theta_{emit}) \tag{3.10}$$

This expression shows the same sin^2 angle dependence as Equation (3.6), and is independent of refractive index. Although refractive index contrast can modify the absolute intensity of light across the interface, this can only increase the short circuit current of a solar cell and not the maximum theoretical efficiency, as with a conventional LSC.[76]

Additionally this scheme does not require a stokes shift of the frequency of the radiation emitted from dipole radiators to minimize light that escapes the device through re-absorption and re-emission. Rather, the efficiency actually benefits from the angular redistribution of the light leaving the device after being emitted from the dipole. Indeed, as pointed out by Rau *et al.,* conventional LSC's cannot provide any efficiency increases over the standard flat-plate efficiency of 33.7% because of the equivalent changes to J_{sc}

and J_o resulting from that mechanism of optical concentration.[76] The scheme proposed here can, in principle, can enable significant efficiency gains over a conventional flat-plate cell.

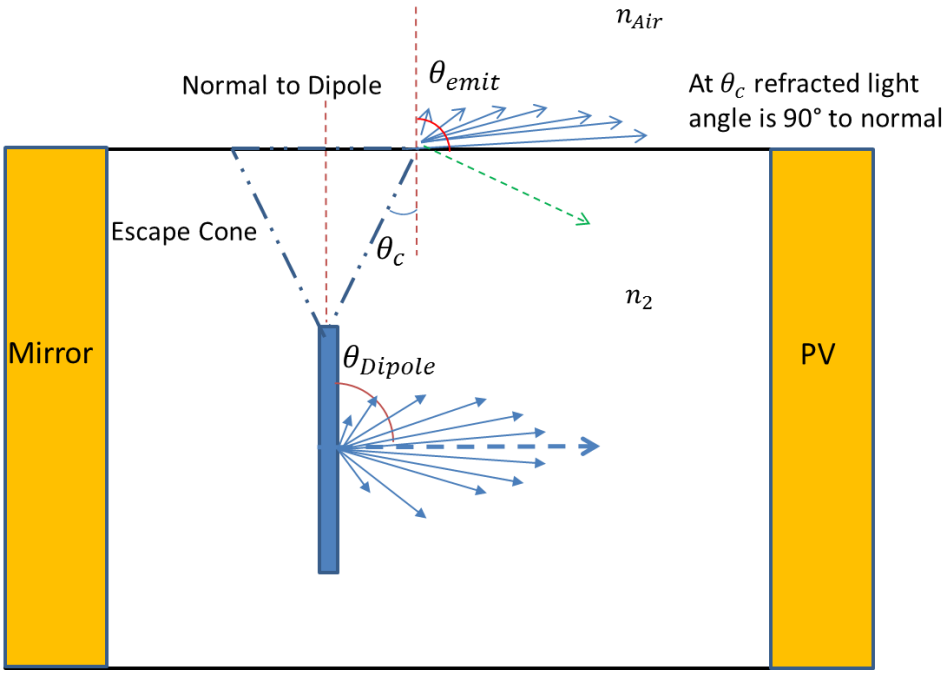

Figure 3.5. Schematic depicting the angular distributions of light exiting a dipole emitter and the emission pattern leaving the device structure.

4. REAL MATERIAL APPLICATIONS

4.1 Gallium Arsenide Cells with Auger Loss

Certainly a single junction solar cell with 60.0% conversion efficiency is an attractive target, but this theoretical efficiency value assumes no non-radiative loss mechanisms. Real semiconducting materials exhibit seemingly unavoidable, more complex loss pathways including Auger recombination, free carrier absorption, and Shockley-Read-Hall recombination, combined with module associated losses such as parasitic absorption from optical components.[69] These additional loss pathways reduce the emitted flux from a cell, and ultra-high efficiency devices require semiconductor materials that have extremely high external radiative efficiencies. Recent single crystalline GaAs cells made by Alta Devices exhibit unprecedented external radiative efficiencies approaching 35%, and have demonstrated power conversion efficiency values of 28.8%, within a few absolute percent of the maximum flat-plate detailed balance limit of 33.7% .[83,84] Although the J_{sc} in these record cells was lower compared to the previous 26.8% efficiency record GaAs cells, the cell V_{oc} was nearly 100 mV larger, confirming that high efficiency cells are excellent light emitters.[83,85] State-of-the-art , defect-free, single crystal GaAs cells have effectively eliminated most non-radiative loss pathways besides Auger recombination and are thus the focus of a more realistic materials-based model for the structured emission strategy outlined in this manuscript.

Adapting the procedure from Kosten *et al.*, the Auger losses in a GaAs cell can be readily accounted for using the detailed balance model by the addition of an Auger recombination term that represents non-radiative energy loss.[46,52]

$$N_{emit}(\theta_{emit}, E, V_{app}, T_{cell})$$

$$= \frac{2\pi}{h^3 c^2} \int_{E_g}^{\infty} \int_{\varphi=0}^{2\pi} \int_{\theta=0}^{\theta_{emit}} I(\theta, E_g) e(\theta, \varphi, E) \frac{E^2}{e^{\left(\frac{E - qV_{app}}{k_b T_{cell}}\right)} - 1} \tag{4.1}$$

$$+ WCn_i^3 e^{\left(\frac{3qV_{app}}{2k_b T_{cell}}\right)} cos\theta sin\theta d\theta d\varphi dE$$

Here W is the cell thickness, C is the Auger coefficient of 7x10^{-30} cm^6 s^{-1}, and n_i is the intrinsic carrier concentration in GaAs.[52,86,87] This expression models a cell with an ideal back reflector so that parasitic absorption losses are neglected.[52] The radiative efficiency of the dipole emitters is also assumed to be ideal, consistent with recent reports of nanorods with unity quantum fluorescence yield.[54] However, optical losses and other non-idealities can be accounted for with additional factors similar to the Auger term, based on the microscopic loss mechanism.[50,52,84] The thickness of the GaAs is 3 μm, which ensures full absorption within the ray optics limit, although the angle dependent emissivity and absorption of the GaAs slab is explicitly accounted for in the calculations.[47,23] The geometry of the modeled PV element is planar, with no surface texturing.

With the use of GaAs as the real material considered for these calculations, the experimentally determined absorptivity and emissivity properties must be included. The absorptivity for a planar GaAs cell with a perfectly reflecting mirror on the rear side can be given by

$$a(\theta, E) = 1 - e^{\left(\frac{-2\alpha(E)W}{cos\theta_p}\right)} \tag{4.2}$$

where $\alpha(E)$ is the experimentally determined absorption coefficient and θ_p is the angle of propagation inside the device after suffering from refraction.[47] Here $cos\theta_p$ can be solved as

$$cos\theta_p = +\sqrt{1 - \frac{1}{n^2}(1 - cos^2\theta_{inc})} \tag{4.3}$$

where $\theta_{inc}$is the incident angle of light on the cell, and n is the refractive index.[47] The assumptions made here are that light enters the surface at normal incidence, $\theta_{inc} = 0$, and that the absorptivity for light emitted is averaged within the emission angle.[46] The absorptivity shown here is adequate for planar GaAs cells and further considerations of modal structuring, as shown by Stuart and Hall[88], need not be considered as light in trapped modes cannot access free space and thus does not contribute to the absorptivity.[46] In calculations for this chapter this form of the absorptivity expression is used explicitly for both absorptivity and emissivity; however, for the emissivity the angle of emission is substituted into Equation (4.3) for θ_{inc}rather than normal incidence.

Inspection of Equations (4.2) and (4.3) show the absorptivity and emissivity of the cell are dependent on the experimentally determined values of refractive index and

absorptivity coefficients for GaAs. Thus, these values were collected from Aspnes and Studna[89] and included in the calculations using Equation (4.1) for real GaAs cells, they are additionally shown plotted as functions of wavelength and energy in Figure 4.1. As expected the absorptivity of GaAs is greatest at large energies and stops absorbing just below its band gap value (1.424 eV), corresponding to a wavelength of 871 nm.

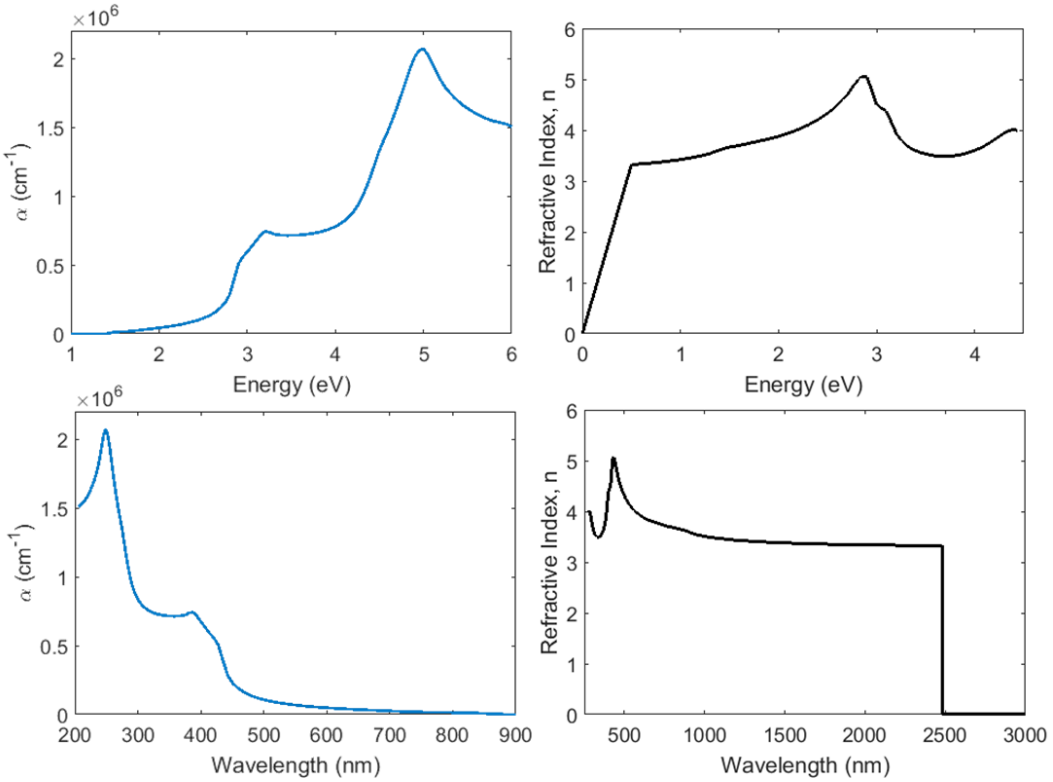

Figure 4.1. Plots of absorption coefficient, α, (left) and refractive index, n, (right) as functions of energy (top) and wavelength (bottom) for GaAs.

Figure 4.2 plots the detailed balance efficiency of GaAs cells with and without Auger losses, also accounting for the combined effects of angle restriction and structured emission provided by dipole radiators. Also shown are the effect of losses (dashed

traces) that may be associated with the optical structure that provides dipole emission combined with Auger losses. The efficiency is plotted versus the angular range of light emission in order to emphasize several benefits resulting from the interaction of these effects. Figure 4.2 (A) indicates that dipolar emission (orange trace) increases the efficiency of the cell with any amount of angular restriction of the emission, with the greatest enhancements observed for the most restricted case (smallest angular range), corresponding to emission into the same angular range as direct sunlight, $\theta_{emit} = \theta_{Sun} = 0.267°$. The additional losses due to Auger recombination, shown in Figure 4.2 (B), significantly limit the maximum theoretical efficiency to a value of 35.88%, though dipole emission (green trace) still provides an improved efficiency for any amount of angle restriction that has not reached this Auger-limited value. Importantly, there is also a decrease in the required amount of angular restriction at which the maximum efficiency is reached, by approximately 12°. The Auger limited cell has a maximum efficiency of ~ 35.8% extending to an angle of 6.9°, while the additional dipole term extends this efficiency to an angle of 18.5 °. By relaxing the requirements for the angular range over which light can exit or enter the device structure, dipolar structured emission allows less extreme angle restriction to realize the same efficiency. Thus a tracking device with a tolerance of up to approximately 19° can provide the same maximum conversion efficiency value of 35.8% for this scheme, as a concentrator or angle restriction device that must track the sun within 7° to maintain maximum efficiency. This benefit could potentially enable less demanding trackers to be used in conjunction with ultrahigh efficiency convertor designs.

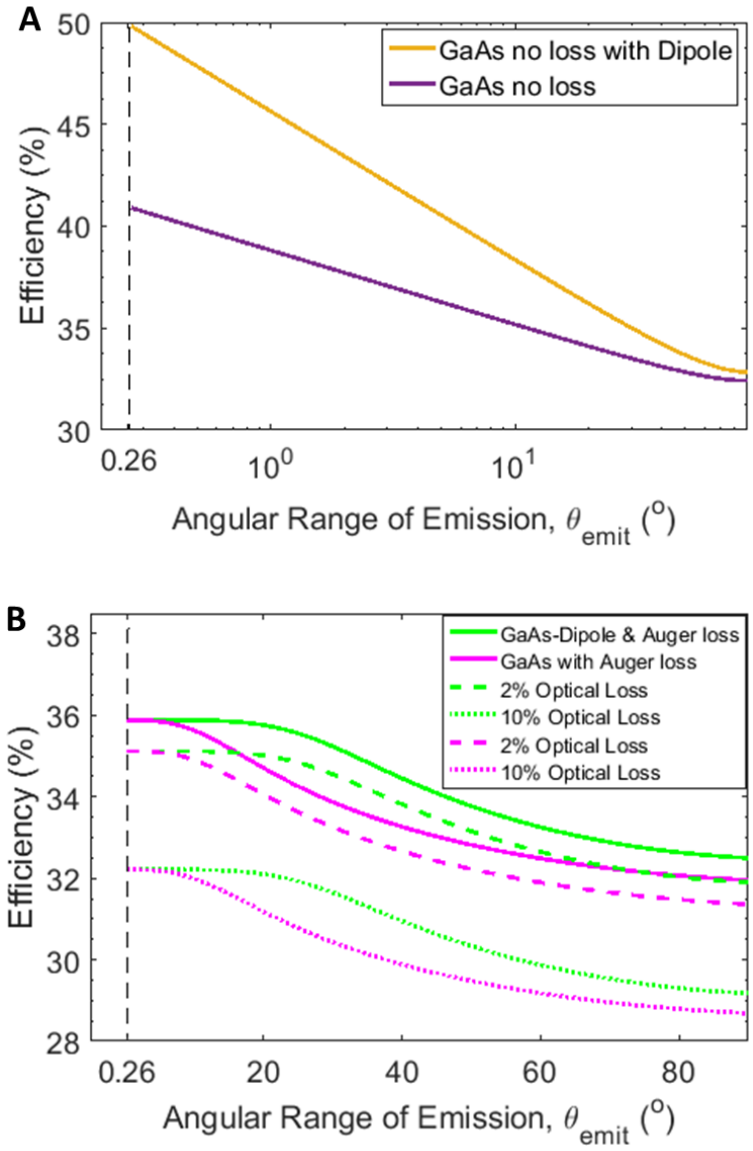

Figure 4.2. Efficiency plot vs the angular range of emitted light for a 3 μm planar GaAs cell, and the same cell with a dipole emission pattern with A) no losses considered and B) Auger recombination losses included, as in Equation (4.1). The dashed lines correspond to varying amounts of optical loss that may also be associated with the structure that provides the dipole emission.

To account for the losses in Figure 4.2 (B) adaptations were made to the procedure from Kosten et al.[52] that was previously used to prove that conversion

efficiency benefits from angular restriction optics are compatible with the external radiative efficiency of high-quality GaAs. Prior to the report from Kosten, Martí and co-workers had argued that angular restriction schemes would not be beneficial in planar GaAs cells, because the ratio of non-radiative to radiative lifetime of 0.1 eliminated any net improvement in performance.[47] The full analysis that refutes Martí's claim will not be repeated here, but instead it is shown that also accounting for optical losses that may be inherent to a coupling structure, such as non-ideal quantum yield from semiconducting nanorods, still can provide benefits for GaAs-based devices.

4.2 Optical Loss Inclusion

Without providing a full ray-tracing analysis, it is considered there is an average optical efficiency for the coupling scheme, such that R times the radiative emission from the cell gives the non-radiative loss due to the coupling optics.[90] This loss is separate from the voltage-dependent losses to Auger recombination (as in Equation (4.1)) and will additionally decrease the amount of sunlight that reaches the PV element. To account for this additional loss, the detailed balance equation can be rewritten as:

$$(1-R)*\int_{\theta=0}^{\theta_{inc}}\int_{E_g}^{\infty} a(\theta,\varphi,E)S(E)\,dEd\theta$$

$$=(1+R)\frac{2\pi}{h^3c^2}\int_{E_g}^{\infty}\int_{\varphi=0}^{2\pi}\int_{\theta=0}^{\theta_{max}} I(\theta,E)e(\theta,\varphi,E)\frac{E^2}{e^{\left(\frac{E-qV_{app}}{k_bT_{cell}}\right)}-1} \tag{4.4}$$

$$+WCn_i^3e^{\left(3qV_{app}/2k_bT_{cell}\right)}cos\theta sin\theta d\varphi d\theta dE$$

As can be seen in Figure 4.3, the additional loss systematically lowers efficiency. However, even with equivalent optical loss, dipole structured emission combined with angle restriction improves performance compared to angle restriction alone. Only when the Auger-limited efficiency is reached, at small angular ranges of emissions, is the efficiency equivalent, though dipole structured emission approaches this maximum efficiency with less severe angle restriction, as discussed in section 4.1. For reference, high quality silvers mirrors exhibit 98% optical efficiency[24,52], and some reported nanorods display fluorescence quantum yield up to 100%, so an optical efficiency above 90% may be compatible with optimized implementations.[54]

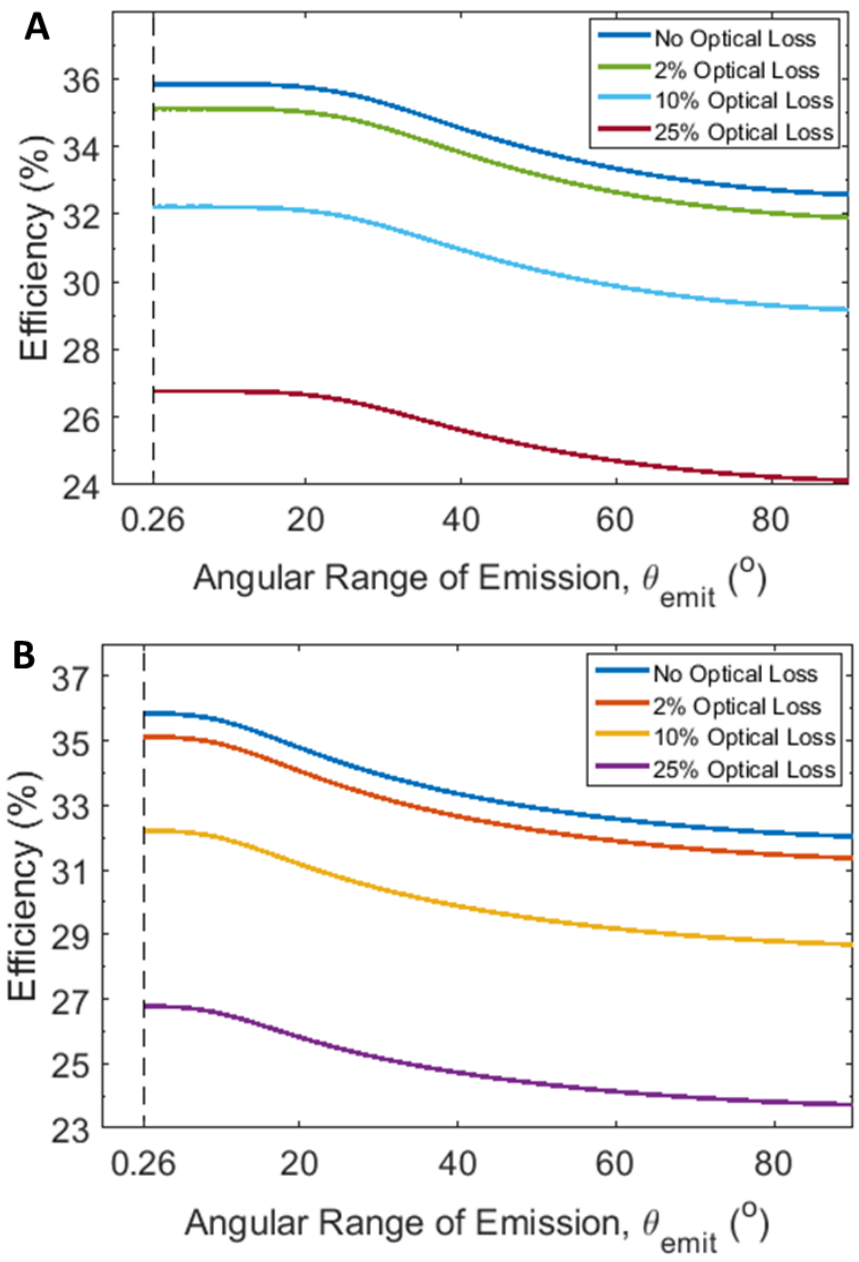

Figure 4.3. The calculated efficiency of a GaAs cell with both Auger losses and losses due to coupling optics with A) angle restriction combined with dipole structured emission and B) angle restriction.

4.3 Limitations When Applying Nanorods as the Dipole Source

Throughout this manuscript the dipole sources responsible for the $\sin^2$ emission restriction have been assumed to be perfect radiators. In contrast to the idealities associated with these perfect sources, they may be replaced with real materials such as dipolar semiconductor nanorods, mentioned in section 3.2, where non-ideal behavior must be included in the calculations. To do so a numerical calculation must be performed by which the band-edge reemission from the nanorods is accounted for. Here the bandwidth of the dipolar absorption and emission into states above the band edge can be implemented and shown how it affects efficiency. While detailed experimental data would be preferred for this implementation, in the absence of data, we may hypothesize that states of polarized emissivity and absorptivity may be related to the bandwidth of the photoluminescence of the nanostructure. The absorptivity, $a(\theta, \varphi, E)$, can then be modified through the same $I(\theta, E_g)$ term from Equation (4.1), but with an explicit bandwidth, ΔE, of dipolar absorptivity above the band edge, with $I(\theta, E_g \rightarrow E_g + \Delta E)$. The bandwidth values considered are based on reported photoluminescence bandwidth values of GaAs.[91,92] Importantly, one must bear in mind that the modified emission is only allowed into the specified energy range above E_g and that the absorption is simultaneously attenuated with the $\sin^2$ modification for observed angles within this same ΔE. Figure 4.4 shows the bandwidth inclusion for an Auger-limited GaAs cell where ΔE = 10, 30, and 70 meV above the E_g of GaAs (1.424 eV). This figure shows a systematic decrease in efficiency as larger ΔE ranges are probed, attributed to the decreased absorptivity of the cell within these ranges. While total efficiency decreases,

the angular range to which the approximate maximum efficiency is unchanged. This trend is analogous to a cell having a larger bandgap and simply absorbing less light. The light lost is reflected in Figure 4.5 where the irradiance and photon flux of the AM 1.5D spectra are shown above E_g (solid blue) and the values of ΔE are shown in the inset by colored lines at their corresponding wavelength, where Table 4.1 displays the respective energy lost in each range above E_g.

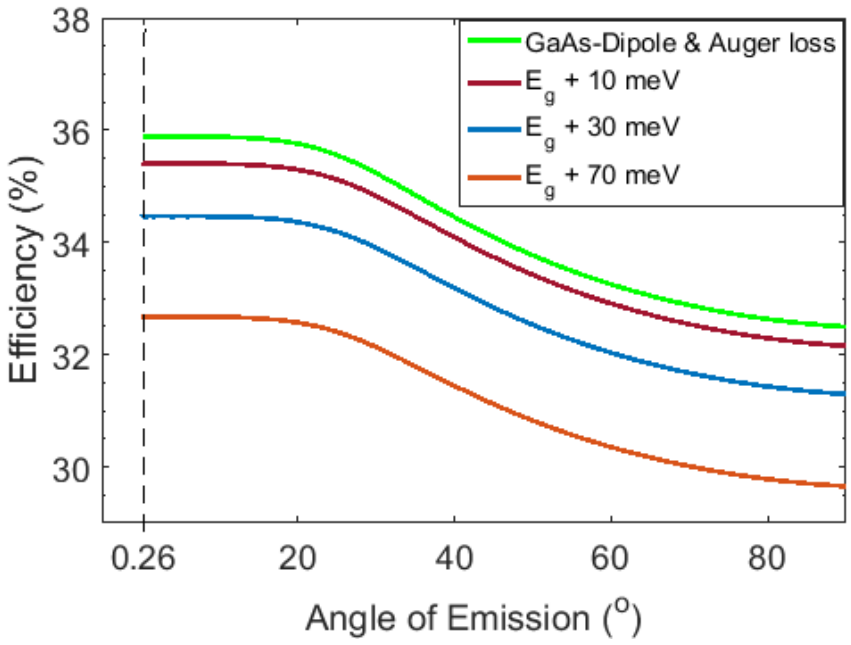

Figure 4.4. The Auger-limited GaAs cell with additional light attenuation considered for realistic nanomaterial absorption and emission just above the GaAs bandgap value of 1.424 eV.

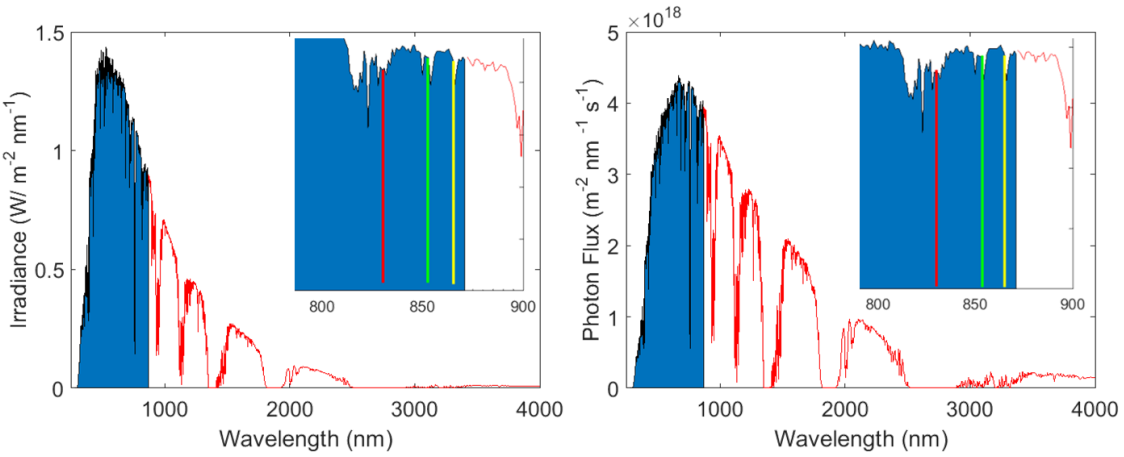

Figure 4.5. Irradiance (left) and photon flux (right) of the AM 1.5D spectra with the amount of energy absorbed shown in blue above the GaAs $\boldsymbol{E_g}$ value which is equivalent to 871 nm. The insets show a magnified view from 800-900 nm where the corresponding $\Delta\boldsymbol{E}$ bandwidth regions probed in Fig. 4.4 are shown for 10 meV (yellow), 30 meV (green), and 70 meV (red).

Table 4.1. Values for each of the bandwidth regions above E_g in Figure 4.5 along with the corresponding region of energy not absorbed by a GaAs cell assuming a cutoff absorption at that value.

$\boldsymbol{E_g}$ **(eV)**	$\Delta\boldsymbol{E}$ **(eV)**	**λ (nm)**	**E Lost (W/m^2)**	**Photons Lost (10^{18})**
1.424	0	871	0	0
1.434	10	865	6.9	26.6
1.454	30	853	16.9	73.3
1.494	70	830	37.7	161.4

Similarly the addition of a ΔE dependence can be applied to the more generalized approach for an arbitrary E_g cell. The modified absorptivity and emissivity as discussed above can be substituted into Equation (3.1) for a nanorod structured emitter for every E_g. In doing so, a very different result is obtained when compared to Figure 3.3. Figure

4.6 (A) plots the efficiency results of a generalized cell with dipole emission and perfect restriction (analogous to Figure 3.2 (D) and Figure 3.3 (blue)) exhibiting only radiative losses, projecting that maximum efficiency is limited to the best case scenario for perfect restriction. Interestingly though, a small efficiency improvement results for a ΔE value of 200 meV with an efficiency of 45.2% at a E_g value of 0.92 eV. This finding will be explored further by investigating the E_g and ΔE ranges at higher accuracy, over a higher count of interval regions, in the near future. Currently the computation time required for this calculation is intensive and thus will be looked into more to validate this result and distinguish it from the possibility of rounding errors potentially present in the simulation; however, if correct this provides a path to efficiency improvement, albeit small improvement, for nanorod materials with a decreased band gap. Beyond the bandwidth range of 200 meV the efficiency begins to decrease overall. While maximum efficiency is no longer significantly improved with the realistic inclusion of nanorod materials, an interesting trend is apparent whereby the E_g at which the maximum occurs is shifted towards lower E_g values. By decreasing the maximum E_g value new materials may be explored with potential benefits of reduced cost and greater absorptivity of low energy light. The values of maximum efficiency and band gap are shown in Table 4.2 for the values in Figure 4.6 (A).

The inclusion of the above mentioned realistic absorptivity and emissivity for dipolar nanorod materials was also included for the non-restricted detailed balance limit, shown in Figure 4.6 (B). The results of this calculation show only a decrease in efficiencies upon the addition of any ΔE value. The trend of lower band gap materials

maintaining the maximum efficiency value is also reflected here, however the decrease in absolute efficiency mitigates the significance of this trend.

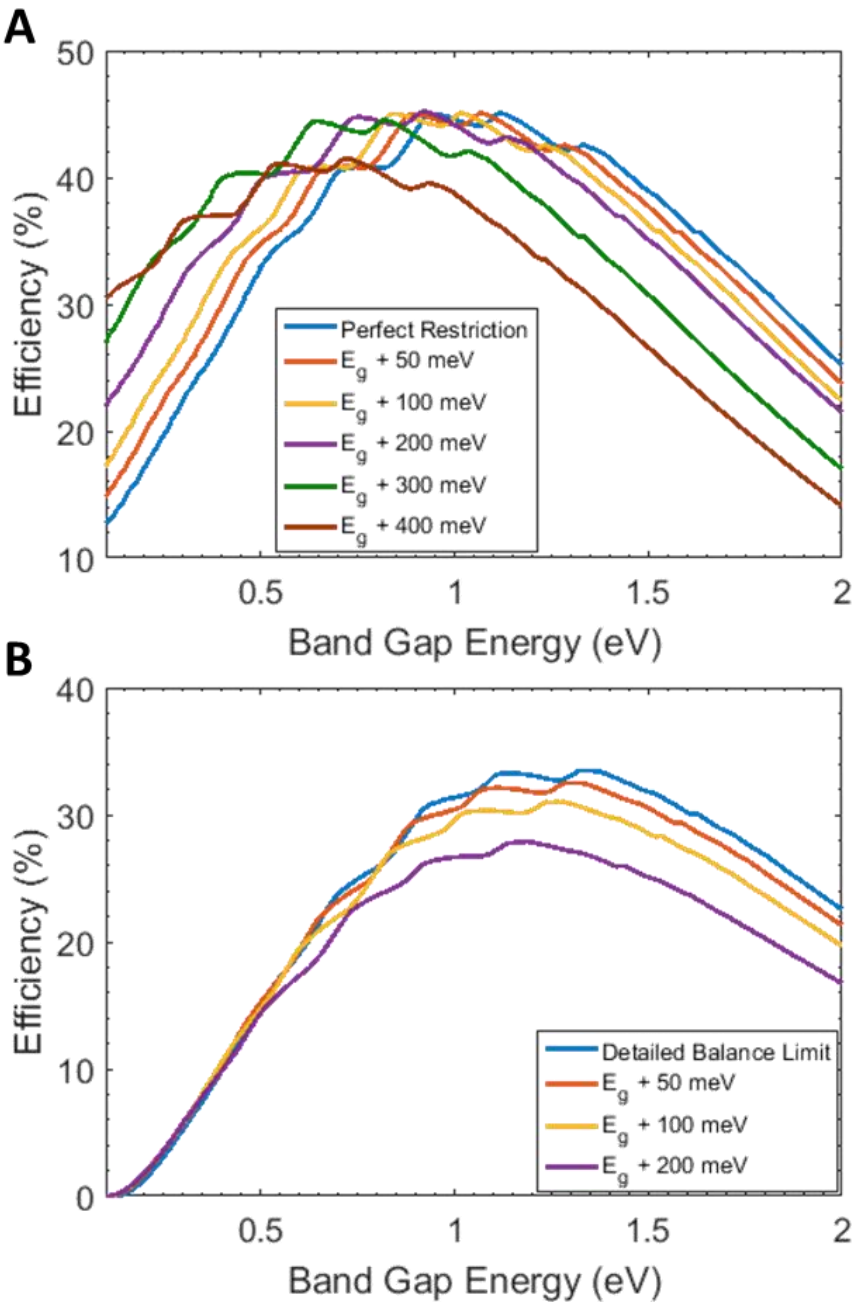

Figure 4.6. Efficiency plots for the A) dipole-restricted case and B) detailed balance case with dipole inclusion. Both plots simulate the real properties derived from nanorod materials with a bandwidth emission range of $\Delta \boldsymbol{E}$.

Table 4.2. The maximum efficiency values reported for the plots shown in Fig. 4.6 (A) which includes nanorod absorption and emission with perfect restriction.

Case	Max Efficiency (%)	E_g (eV)
Perfect Restriction	45.06	1.12
E_g + 50 meV	45.05	1.06
E_g + 100 meV	45.06	1.02
E_g + 200 meV	45.20	0.92
E_g + 300 meV	44.52	0.82
E_g + 400 meV	41.50	0.72

5. CONCLUSION

This thesis applied the use of the detailed balance method to a theoretical PV device relying on angle restriction to improve the overall efficiency of the cell. We have demonstrated that the maximum efficiency of a solar cell can be increased by modifying the angular dependent emission pattern of radiation leaving the device. We specifically consider the improvement provided by highly efficient dipole radiators. When placed optically in-series with the photovoltaic element, dipole radiators provide a $\sin^2$ intensity distribution of emitted radiation. Accounting for this structured emission using the detailed balance method for calculating conversion efficiency results in a 0.6% absolute improvement compared with a solar cell that emits radiation isotropically. Combining structured emission with angle restriction optics further increases the maximum theoretical efficiency to a value of 60.0%.

Analysis of non-radiative Auger losses in high-efficiency 3 μm planar GaAs cells indicates that systematic efficiency improvements can be anticipated in realistic device implementations, while simultaneously relaxing requirements for solar trackers. Even when optical losses, inherent in most real systems, are included the angles to which maximum efficiencies correspond are increased compared to non-restricted calculations. We envision that this strategy can be further improved if efficient radiators with higher order multipoles, or other arbitrary radiations patterns, can be developed to more effectively structure the optical emission from solar cells and promote increased light trapping.

Finally semiconductor nanocrystals were included in the calculations, simulating realistic absorption and emission properties for GaAs nanorod materials. Auger-limited GaAs cells continued to show dominant losses due to non-radiative auger emission, while systematically decreasing in efficiency as larger bandwidth regions were probed. In the Auger-limited case the cell behaved similarly to increasing the band gap of the cell whereby efficiency decreased as the count of photons absorbed decreased close to the bandgap of the cell. Additionally, the decreased absorptivity and restricted emissivity within a range of bandwidths was simulated for the detailed balance efficiency of arbitrary band gap values. It was shown that the traditional perfect restriction maximum efficiency was the limiting efficiency. Although no significant efficiency improvements were achieved, a shift to lower band gap values occurred for the maximum efficiency point. While these results may be limiting for the case of semiconductor nanomaterials they show interesting trends in maximum efficiency band gap shifts that are encouraging for the exploration of reduced band gap materials with reduced cost and increased absorptivity.

REFERENCES

1. International Energy Agency. *Excerpt from Renewables Information*; [Online] April **2016**. http://www.iea.org/bookshop/728-Renewables_Information_2016 (accessed July 13, 2016).

2. Lewis, N. S.; Nocera, D. G., Powering the planet: Chemical challenges in solar energy utilization. *Proceedings of the National Academy of Sciences* **2006,** *103* (43), 15729-15735.

3. U.S. Department of Energy. *Sunshot Vision Study: Photovoltaic System Pricing Trends-Historical, Recent, and Near-Term Projections;* National Renewable Energy Laboratory: Golden, CO, **2014**.

4. U.S. Energy Information Administration. *Electric Power Monthly: Information for May 2016*; [Online] May 25, **2016**. http://www.eia.gov/totalenergy/data/monthly/archive/00351605.pdf (accessed July 15, 2016)

5. Reichelstein, S.; Sahoo, A. *Cost- and Price Dynamics of Solar PV Modules*; Stanford University; [Online] November **2015**. https://www-cdn.law.stanford.edu/wp-content/uploads/2015/06/Reichelstein-Sahoo-CostandPriceRevision-Nov2015.pdf (accessed August 12, 2016).

6. Lang, J., *New efficiency record for a commercial-scale solar cell module arrives in the form of a flexible thin film semiconductor*. Yale Climate and Energy Institute News Release; [Online] March 13, **2013**. http://climate.yale.edu/news/new-efficiency-record-commercial-scale-solar-cell-module-arrives-form-flexible-thin-film (accessed August 12, 2016).

7. Masuko, K.; Shigematsu, M.; Hashiguchi, T.; Fujishima, D.; Kai, M.; Yoshimura, N.; Yamaguchi, T.; Ichihashi, Y.; Mishima, T.; Matsubara, N.; Yamanishi, T.; Takahama, T.; Taguchi, M.; Maruyama, E.; Okamoto, S., Achievement of More Than 25%; Conversion Efficiency With Crystalline Silicon Heterojunction Solar Cell. *IEEE Journal of Photovoltaics* **2014,** *4* (6), 1433-1435.

8. National Renewable Energy Laboratory (NREL), Golden, CO. Best Research-Cell Efficiency Chart. [Online] **2016**. http://www.nrel.gov/pv/national-center-for-photovoltaics.html (accessed September 22, 2016).

9. Aberle, A. G., Thin-film solar cells. *Thin Solid Films* **2009,** *517* (17), 4706-4710.

10. Bloss, W. H.; Pfisterer, F.; Schubert, M.; Walter, T., Thin-film solar cells. *Progress in Photovoltaics: Research and Applications* **1995,** *3* (1), 3-24.

11. Chiu, P. T.; Law, D. C.; Woo, R. L.; Singer, S. B.; Bhusari, D.; Hong, W. D.; Zakaria, A.; Boisvert, J.; Mesropian, S.; King, R. R.; Karam, N. H. *35.8% space and 38.8% terrestrial 5J direct bonded cells*, 2014 IEEE 40th Photovoltaic Specialist Conference (PVSC), 8-13 June 2014; 2014; pp 0011-0013.

12. Dimroth, F.; Grave, M.; Beutel, P.; Fiedeler, U.; Karcher, C.; Tibbits, T. N. D.; Oliva, E.; Siefer, G.; Schachtner, M.; Wekkeli, A.; Bett, A. W.; Krause, R.; Piccin, M.; Blanc, N.; Drazek, C.; Guiot, E.; Ghyselen, B.; Salvetat, T.; Tauzin, A.; Signamarcheix, T.; Dobrich, A.; Hannappel, T.; Schwarzburg, K., Wafer bonded four-junction GaInP/GaAs//GaInAsP/GaInAs concentrator solar cells with 44.7% efficiency. *Progress in Photovoltaics: Research and Applications* **2014,** *22* (3), 277-282.

13. King, R. R.; Boca, A.; Hong, W.; Law, D.; Kinsey, G.; Fetzer, C.; Haddad, M.; Edmondson, K.; Yoon, H.; Pien, P.; Karam, N. *High-efficiency multijunction photovoltaics for low-cost solar electricity*, 21st Annual Meeting of the IEEE Lasers and Electro-Optics Society. Nov. 9-13, **2008**; pp 2-3.

14. Schneider, K., *New world record for solar cell efficiency at 46%*. Fraunhofer Institute for Solar Energy Systems ISE: Freiburg Germany, **2014**.

15. Swanson, R. M., The promise of concentrators. *Progress in Photovoltaics: Research and Applications* **2000,** *8* (1), 93-111.

16. Munday, J. N., The effect of photonic bandgap materials on the Shockley-Queisser limit. *Journal of Applied Physics* **2012,** *112* (6), 064501.

17. Callahan, D. M.; Munday, J. N.; Atwater, H. A., Solar Cell Light Trapping beyond the Ray Optic Limit. *Nano Letters* **2012,** *12* (1), 214-218.

18. Ulbrich, C.; Peters, M.; Bläsi, B.; Kirchartz, T.; Gerber, A.; Rau, U., Enhanced light trapping in thin-film solar cells by a directionally selective filter. *Opt. Express* **2010,** *18* (S2), A133-A138.

19. Deckman, H. W.; Wronski, C. R.; Witzke, H.; Yablonovitch, E., Optically enhanced amorphous silicon solar cells. *Applied Physics Letters* **1983,** *42* (11), 968-970.

20. Ulbrich, C.; Fahr, S.; Üpping, J.; Peters, M.; Kirchartz, T.; Rockstuhl, C.; Wehrspohn, R.; Gombert, A.; Lederer, F.; Rau, U., Directional selectivity and ultra-light-trapping in solar cells. *physica status solidi (a)* **2008,** *205* (12), 2831-2843.

21. Polman, A.; Atwater, H. A., Photonic design principles for ultrahigh-efficiency photovoltaics. *Nat Mater* **2012,** *11* (3), 174-7.

22. Yablonovitch, E., Statistical ray optics. *J. Opt. Soc. Am.* **1982,** *72* (7), 899-907.

23. Yablonovitch, E.; Cody, G. D., Intensity enhancement in textured optical sheets for solar cells. *Electron Devices, IEEE Transactions on* **1982,** *29* (2), 300-305.

24. Kuhn, H.; Wilson, B. A., Reflectivity of thin silver films and their use in interferometry. *Proceedings of the Physical Society. Section B* **1950,** *63* (10), 745.

25. Schuller, J. A.; Barnard, E. S.; Cai, W.; Jun, Y. C.; White, J. S.; Brongersma, M. L., Plasmonics for extreme light concentration and manipulation. *Nat Mater* **2010,** *9* (3), 193-204.

26. Atwater, H. A.; Polman, A., Plasmonics for improved photovoltaic devices. *Nat Mater* **2010,** *9* (3), 205-213.

27. Xu, Y.; Munday, J. N., Light trapping in a polymer solar cell by tailored quantum dot emission. *Opt. Express* **2014,** *22* (S2), A259-A267.

28. Nozik, A. J., Quantum dot solar cells. *Physica E: Low-dimensional Systems and Nanostructures* **2002,** *14* (1–2), 115-120.

29. Ross, R. T.; Nozik, A. J., Efficiency of hot-carrier solar energy converters. *Journal of Applied Physics* **1982,** *53* (5), 3813-3818.

30. Brongersma, M. L.; Cui, Y.; Fan, S., Light management for photovoltaics using high-index nanostructures. *Nat Mater* **2014,** *13* (5), 451-460.

31. Protesescu, L.; Yakunin, S.; Bodnarchuk, M. I.; Krieg, F.; Caputo, R.; Hendon, C. H.; Yang, R. X.; Walsh, A.; Kovalenko, M. V., Nanocrystals of Cesium Lead Halide Perovskites (CsPbX3, X = Cl, Br, and I): Novel Optoelectronic Materials Showing Bright Emission with Wide Color Gamut. *Nano Letters* **2015,** *15* (6), 3692-3696.

32. Shockley, W.; Queisser, H. J., Detailed Balance Limit of Efficiency of p-n Junction Solar Cells. *Journal of Applied Physics* **1961,** *32* (3), 510-519.

33. Standard Tables for Reference Solar Spectral Irradiances: Direct Normal and Hemispherical on 37°; Tilted Surface. ASTM International: **2012**.

34. Parry-Hill, M. J.; Sutter, R. T.; Davidson, M. W., [image credit] Figure 1. *Electron and Current Flow In Solar Cells*. Florida State University. Molecular Expressions: Optical Microscopy Primer: Physics of light and color: Light and Color: Light and Energy: Solar Cell Operation, **2015**. https://micro.magnet.fsu.edu/primer/java/solarcell/index.html (accessed April 2016).

35. Nelson, J., *The Physics of Solar Cells*. Imperial College Press: London England, **2003**; p 4-21.

36. Siegel, R.; Howell, J. R., *Thermal Radiation and Heat Transfer*. 2nd ed.; Hemisphere Publishing Corporation: Washington D.C., **1981**; p 10-45.

37. Luque, A.; Marti, A., *Handbook of Photovoltaic Science and Engineering, Chapter 4: Theoretical Limits of Photovoltaic Conversion*. 2nd ed.; John Wiley & Sons: **2011**.

38. Xu, Y.; Gong, T.; Munday, J. N., The generalized Shockley-Queisser limit for nanostructured solar cells. *Scientific Reports* **2015,** *5*, 13536.

39. Lacis, A. A.; Hansen, J., A Parameterization for the Absorption of Solar Radiation in the Earth's Atmosphere. *Journal of the Atmospheric Sciences* **1974,** *31* (1), 118-133.

40. Honsberg, C.; Bowden, S., Chapter 2. Properties of Sunlight, 2.4 Terrestrial Solar Radiation: Air Mass. Photovoltaic Education Network: **2014**.

41. Emery, K.; Myers, D.; Kurtz, S. In *What is the appropriate reference spectrum for characterizing concentrator cells?*, Photovoltaic Specialists Conference, 2002. Conference Record of the Twenty-Ninth IEEE, 19-24 May **2002**; pp 840-843.

42. Xu, Y.; Munday, J. N., Designing Photonic Materials for Effective Bandgap Modification and Optical Concentration in Photovoltaics. *IEEE Journal of Photovoltaics* **2014,** *4* (1), 233-236.

43. Vossier, A.; Gualdi, F.; Dollet, A.; Ares, R.; Aimez, V., Approaching the Shockley-Queisser limit: General assessment of the main limiting mechanisms in photovoltaic cells. *Journal of Applied Physics* **2015,** *117* (1), 015102.

44. Mann, S. A.; Grote, R. R.; Osgood, R. M.; Alù, A.; Garnett, E. C., Opportunities and Limitations for Nanophotonic Structures To Exceed the Shockley–Queisser Limit. *ACS Nano* **2016**.

45. Green, M. A., *Solar cells : Operating Principles, Technology, and System Applications. Martin A. Green*. Englewood Cliffs, N.J. : Prentice-Hall: **1982**.

46. Kosten, E. D. Optical Designs for Improved Solar Cell Performance. California Institute of Technology, Pasadena, California, **2014**.

47. Martí, A.; Balenzategui, J. L.; Reyna, R. F., Photon recycling and Shockley's diode equation. *Journal of Applied Physics* **1997,** *82* (8), 4067-4075.

48. Peters, M.; Goldschmidt, J. C.; Bläsi, B., Angular confinement and concentration in photovoltaic converters. *Solar Energy Materials and Solar Cells* **2010,** *94* (8), 1393-1398.

49. Rau, U.; Paetzold, U. W.; Kirchartz, T., Thermodynamics of light management in photovoltaic devices. *Physical Review B* **2014,** *90* (3), 035211.

50. Kosten, E. D.; Kayes, B. M.; Atwater, H. A., Experimental demonstration of enhanced photon recycling in angle-restricted GaAs solar cells. *Energy & Environmental Science* **2014,** *7* (6), 1907-1912.

51. Braun, A.; Katz, E. A.; Feuermann, D.; Kayes, B. M.; Gordon, J. M., Photovoltaic performance enhancement by external recycling of photon emission. *Energy & Environmental Science* **2013,** *6* (5), 1499-1503.

52. Kosten, E. D.; Atwater, J. H.; Parsons, J.; Polman, A.; Atwater, H. A., Highly efficient GaAs solar cells by limiting light emission angle. *Light Sci Appl* **2013,** *2*, e45.

53. Munday, J. N., The effect of photonic bandgap materials on the Shockley-Queisser limit. *Journal of Applied Physics* **2012,** *112* (6).

54. Coropceanu, I.; Rossinelli, A.; Caram, J. R.; Freyria, F. S.; Bawendi, M. G., Slow-Injection Growth of Seeded CdSe/CdS Nanorods with Unity Fluorescence Quantum Yield and Complete Shell to Core Energy Transfer. *ACS Nano* **2016**.

55. Yin, Y.; Alivisatos, A. P., Colloidal nanocrystal synthesis and the organic-inorganic interface. *Nature* **2005,** *437* (7059), 664-670.

56. Milliron, D. J.; Hughes, S. M.; Cui, Y.; Manna, L.; Li, J.; Wang, L.-W.; Paul Alivisatos, A., Colloidal nanocrystal heterostructures with linear and branched topology. *Nature* **2004,** *430* (6996), 190-195.

57. Hu, J.; Li, L.-s.; Yang, W.; Manna, L.; Wang, L.-w.; Alivisatos, A. P., Linearly Polarized Emission from Colloidal Semiconductor Quantum Rods. *Science* **2001,** *292* (5524), 2060-2063.

58. Mulder, C. L.; Reusswig, P. D.; Velázquez, A. M.; Kim, H.; Rotschild, C.; Baldo, M. A., Dye alignment in luminescent solar concentrators: I. Vertical alignment for improved waveguide coupling. *Opt. Express* **2010,** *18* (S1), A79-A90.

59. Bronstein, N. D.; Li, L.; Xu, L.; Yao, Y.; Ferry, V. E.; Alivisatos, A. P.; Nuzzo, R. G., Luminescent Solar Concentration with Semiconductor Nanorods and Transfer-Printed Micro-Silicon Solar Cells. *ACS Nano* **2013,** *8* (1), 44-53.

60. Bradshaw, L. R.; Knowles, K. E.; McDowall, S.; Gamelin, D. R., Nanocrystals for Luminescent Solar Concentrators. *Nano Letters* **2015,** *15* (2), 1315-1323.

61. Diroll, B. T.; Dadosh, T.; Koschitzky, A.; Goldman, Y. E.; Murray, C. B., Interpreting the Energy-Dependent Anisotropy of Colloidal Nanorods Using Ensemble and Single-Particle Spectroscopy. *The Journal of Physical Chemistry C* **2013,** *117* (45), 23928-23937.

62. Diroll, B. T.; Koschitzky, A.; Murray, C. B., Tunable Optical Anisotropy of Seeded CdSe/CdS Nanorods. *The Journal of Physical Chemistry Letters* **2014,** *5* (1), 85-91.

63. Green, M. A., Time-Asymmetric Photovoltaics. *Nano Letters* **2012,** *12* (11), 5985-5988.

64. Ferraioli, L.; Maddalena, P.; Massera, E.; Parretta, A.; Green, M. A.; Wang, A.; Zhao, J., Evidence for generalized Kirchhoff's law from angle-resolved electroluminescence of high efficiency silicon solar cells. *Applied Physics Letters* **2004,** *85* (13), 2484-2486.

65. Rau, U.; Kirchartz, T., The Principle of Detailed Balance and the Opto-Electronic Properties of Solar Cells. In *Photon Management in Solar Cells*, Wiley-VCH Verlag GmbH & Co. KGaA: 2015; pp 21-48.

66. Green, M. A., Limits on the open-circuit voltage and efficiency of silicon solar cells imposed by intrinsic Auger processes. *Ieee T Electron Dev* **1984,** *31* (5), 671-678.

67. Araújo, G. L.; Martí, A., Absolute limiting efficiencies for photovoltaic energy conversion. *Solar Energy Materials and Solar Cells* **1994,** *33* (2), 213-240.

68. Parrott, J. E., Thermodynamics of solar cell efficiency. *Solar Energy Materials and Solar Cells* **1992,** *25* (1), 73-85.

69. Niv, A.; Abrams, Z. R.; Gharghi, M.; Gladden, C.; Zhang, X., Overcoming the bandgap limitation on solar cell materials. *Applied Physics Letters* **2012,** *100* (8), 083901.

70. Baruch, P.; De Vos, A.; Landsberg, P. T.; Parrott, J. E., On some thermodynamic aspects of photovoltaic solar energy conversion. *Solar Energy Materials and Solar Cells* **1995,** *36* (2), 201-222.

71. Doeleman, H. Limiting and realistic efficiencies of multi-junction solar cells. FOM Institute AMOLF, Amsterdam, Netherlands, **2012**.

72. Roxlo, C. B.; Yablonovitch, E., Thermodynamics of daylight-pumped lasers. *Opt. Lett.* **1983,** *8* (5), 271-273.

73. van Roosbroeck, W.; Shockley, W., Photon-Radiative Recombination of Electrons and Holes in Germanium. *Physical Review* **1954,** *94* (6), 1558-1560.

74. Wadia, C.; Alivisatos, A. P.; Kammen, D. M., Materials Availability Expands the Opportunity for Large-Scale Photovoltaics Deployment. *Environmental Science & Technology* **2009,** *43* (6), 2072-2077.

75. Chuang, C.-H. M.; Brown, P. R.; Bulović, V.; Bawendi, M. G., Improved performance and stability in quantum dot solar cells through band alignment engineering. *Nat Mater* **2014,** *13* (8), 796-801.

76. Rau, U.; Einsele, F.; Glaeser, G. C., Efficiency limits of photovoltaic fluorescent collectors. *Applied Physics Letters* **2005,** *87* (17), 171101.

77. Liu, Q.; Cui, Y.; Gardner, D.; Li, X.; He, S.; Smalyukh, I. I., Self-Alignment of Plasmonic Gold Nanorods in Reconfigurable Anisotropic Fluids for Tunable Bulk Metamaterial Applications. *Nano Letters* **2010,** *10* (4), 1347-1353.

78. Wang, Y. L.; Chen, L. Y.; Liu, Q. K.; Cai, F. H.; Qian, J., The ordering alignment of gold nanorods in liquid crystals and its applications to polarization-sensitive SERS. *Journal of Physics: Conference Series* **2016,** *680* (1), 012021.

79. Baker, J. L.; Widmer-Cooper, A.; Toney, M. F.; Geissler, P. L.; Alivisatos, A. P., Device-Scale Perpendicular Alignment of Colloidal Nanorods. *Nano Letters* **2010,** *10* (1), 195-201.

80. Ahmed, W.; Kooij, E. S.; van Silfhout, A.; Poelsema, B., Quantitative Analysis of Gold Nanorod Alignment after Electric Field-Assisted Deposition. *Nano Letters* **2009,** *9* (11), 3786-3794.

81. Debije, M. G.; Verbunt, P. P. C., Thirty Years of Luminescent Solar Concentrator Research: Solar Energy for the Built Environment. *Advanced Energy Materials* **2012,** *2* (1), 12-35.

82. Sark, W. G. J. H. M. v.; Barnham, K. W. J.; Slooff, L. H.; Chatten, A. J.; Büchtemann, A.; Meyer, A.; McCormack, S. J.; Koole, R.; Farrell, D. J.; Bose, R.; Bende, E. E.; Burgers, A. R.; Budel, T.; Quilitz, J.; Kennedy, M.; Meyer, T.; Donegá, C. D. M.; Meijerink, A.; Vanmaekelbergh, D., Luminescent Solar Concentrators - A review of recent results. *Opt. Express* **2008,** *16* (26), 21773-21792.

83. Green, M. A.; Emery, K.; Hishikawa, Y.; Warta, W.; Dunlop, E. D., Solar cell efficiency tables (version 46). *Progress in Photovoltaics: Research and Applications* **2015,** *23* (7), 805-812.

84. Miller, O. D.; Yablonovitch, E.; Kurtz, S. R., Strong Internal and External Luminescence as Solar Cells Approach the Shockley–Queisser Limit. *Photovoltaics, IEEE Journal of* **2012,** *2* (3), 303-311.

85. Green, M. A., Radiative efficiency of state-of-the-art photovoltaic cells. *Progress in Photovoltaics: Research and Applications* **2012,** *20* (4), 472-476.

86. Araujo, G. L.; Marti, A. In *Limiting efficiency of GaAs solar cells*, Photovoltaic Specialists Conference, 1988., Conference Record of the Twentieth IEEE, **1988**; pp 672-677 vol.1.

87. Strauss, U.; Rühle, W. W.; Köhler, K., Auger recombination in intrinsic GaAs. *Applied Physics Letters* **1993,** *62* (1), 55-57.

88. Stuart, H. R.; Hall, D. G., Thermodynamic limit to light trapping in thin planar structures. *J. Opt. Soc. Am. A* **1997,** *14* (11), 3001-3008.

89. Aspnes, D. E.; Studna, A. A., Dielectric functions and optical parameters of Si, Ge, GaP, GaAs, GaSb, InP, InAs, and InSb from 1.5 to 6.0 eV. *Physical Review B* **1983,** *27* (2), 985-1009.

90. Ross, R. T., Some Thermodynamics of Photochemical Systems. *The Journal of Chemical Physics* **1967,** *46* (12), 4590-4593.

91. Yang, D.; Garland, J. W.; Raccah, P. M.; Coluzza, C.; Frankl, P.; Capizzi, M.; Chambers, F.; Devane, G., Electroreflectance and photoluminescence measurement of passivation by hydrogenation in GaAs/AlGaAs structures. *Physica B: Condensed Matter* **1991,** *170* (1), 557-560.

92. Ihn, S.-G.; Ryu, M.-Y.; Song, J.-I., Optical properties of undoped, Be-doped, and Si-doped wurtzite-rich GaAs nanowires grown on Si substrates by molecular beam epitaxy. *Solid State Communications* **2010,** *150* (15–16), 729-733.